NASA TECHNICAL NOTE

NASA TN D-5232

WIND-TUNNEL INVESTIGATION OF STEADY-STATE AERODYNAMICS OF A COMPOSITE-LIFT VTOL AIRCRAFT MODEL

by Matthew M. Winston and Robert J. Huston

Langley Research Center

Langley Station, Hampton, Va.

NATIONAL AERONAUTICS AND SPACE ADMINISTRATION • WASHINGTON, D. C. • JUNE 1969

NASA TN D-5232

WIND-TUNNEL INVESTIGATION OF STEADY-STATE AERODYNAMICS OF A COMPOSITE-LIFT VTOL AIRCRAFT MODEL

By Matthew M. Winston and Robert J. Huston

Langley Research Center

Langley Station, Hampton, Va.

NATIONAL AERONAUTICS AND SPACE ADMINISTRATION

For sale by the Clearinghouse for Federal Scientific and Technical Information
Springfield, Virginia 22151 – CFSTI price $3.00

WIND-TUNNEL INVESTIGATION OF STEADY-STATE AERODYNAMICS OF A COMPOSITE-LIFT VTOL AIRCRAFT MODEL

By Matthew M. Winston and Robert J. Huston
Langley Research Center

SUMMARY

An investigation of a composite-lift VTOL aircraft model with three different rotor/wing configurations was conducted in the Langley full-scale tunnel. The aircraft configuration was one which employed a three-bladed lifting rotor for helicopter flight which could be stopped to become a fixed wing for airplane cruise flight. The aerodynamic and control characteristics were obtained for helicopter flight and the cruise aerodynamics were obtained for airplane flight.

The results indicate only small differences between the three configurations for most of the helicopter-mode operating conditions. Need for improvements in blade design is indicated, and a potential roll control problem at high tip-speed ratios is identified.

The results of the airplane-mode cruise investigation indicate the importance of careful design of composite lifting surfaces in order to achieve good efficiency in both rotary-wing and fixed-wing flight.

INTRODUCTION

Efforts are underway to develop composite-lift aircraft which combine the high hovering efficiency of the helicopter with the high cruise efficiency of fixed-wing aircraft. Most of the composite-lift vehicles are based on independent lift systems where attempts are made to optimize the hover and cruise systems independently.

One concept, however, combines the hover and cruise systems into a single lifting surface in an attempt to reduce the weight penalty associated with independent systems. For the helicopter flight mode the lifting surface rotates, and for the airplane cruise flight mode the lifting surface is stopped and becomes a fixed wing. Consequently, the lifting surface is generally called the "rotor/wing."

In order to provide some general information on the characteristics of the rotor/wing aircraft, an investigation was undertaken in the Langley full-scale tunnel where a model of the aircraft was investigated in all of its flight modes. Rotor/wing

dynamic stability problems associated with the conversion maneuver are reported in reference 1. The present report presents the steady-state aerodynamic characteristics of the rotor/wing aircraft in the helicopter and airplane flight modes. Three different configurations are compared throughout this investigation.

SYMBOLS

The physical quantities defined in this section are given in both U.S. Customary Units and the International System of Units (SI). Factors relating the two systems are given in reference 2.

A_1 coefficient of $-\cos\psi$ in expression for θ, degrees

A_2 coefficient of $-\cos 2\psi$ in expression for θ, degrees

B_1 coefficient of $-\sin\psi$ in expression for θ, degrees

B_2 coefficient of $-\sin 2\psi$ in expression for θ, degrees

b wing span, feet (meters)

C_D airplane drag coefficient, $\frac{\text{Drag}}{qS}$

C'_D helicopter drag coefficient, $\frac{\text{Drag}}{\pi R^2\rho(\Omega R)^2}$

C_L airplane lift coefficient, $\frac{\text{Lift}}{qS}$

C'_L helicopter lift coefficient, $\frac{\text{Lift}}{\pi R^2\rho(\Omega R)^2}$

C'_l helicopter rolling-moment coefficient, $\frac{\text{Rolling moment}}{\pi R^2\rho(\Omega R)^2 R}$

C_m airplane pitching-moment coefficient, $\frac{\text{Pitching moment}}{qS\bar{c}}$

C'_m helicopter pitching-moment coefficient, $\frac{\text{Pitching moment}}{\pi R^2\rho(\Omega R)^2 R}$

C_Q rotor torque coefficient, $\frac{\text{Torque}}{\pi R^2\rho(\Omega R)^2 R}$

C_T rotor thrust coefficient, $\frac{\text{Thrust}}{\pi R^2\rho(\Omega R)^2}$

$\bar{c}$ wing average chord, S/b, feet (meters)

M rotor figure of merit, $\frac{0.707C_T^{3/2}}{C_Q}$

q free-stream dynamic pressure, pounds force per foot^2 (newtons per meter^2)

R rotor radius, feet (meters)

S wing planform area (based on area of hub and two blades), feet^2 (meters^2)

V velocity, feet per second (meters per second)

α model angle of attack referenced to wing chord plane, degrees

θ_0 rotor blade collective pitch angle used as constant in expression for θ, degrees

θ blade pitch angle at particular azimuth position, $\theta_0 - A_1 \cos \psi - B_1 \sin \psi - A_2 \cos 2\psi - B_2 \sin 2\psi - \ldots$, degrees

ρ mass density of air, slugs per foot^3 (kilograms per meter^3)

ψ blade azimuth angle measured from downwind position in direction or rotation, degrees or radians

Ω rotor rotational speed, radians per second

MODEL AND INSTRUMENTATION

Model

Drawings of the model are given in figure 1, a photograph of the model mounted in the Langley full-scale tunnel is given as figure 2, and model details are listed in table I.

The fuselage was a wood-covered aluminum structural box which contained the rotor/wing support members and the drive and control mechanisms. The aft fuselage section was fitted with a vertical tail and included provisions for a variable-incidence horizontal tail. Only the characteristics of the model with the horizontal tail off, however, are included herein.

Sketches of the three rotor/wings and details of the cross sections are given in figures 3, 4, and 5. All rotors were of equal diameter. The hub of configuration 1 had convex curvature between the three constant-chord blades, the hub of configuration 2 had straight sides connecting three tapered blades, and the hub of configuration 3 had concave curvature between three tapered blades. Consequently, the surface area of each configuration was different. The blades were composed of biconvex airfoil sections with parabolic leading and trailing edges. These sections were symmetrical about both the chord line and the midchord point. The blades were attached to the hub through feathering bearings; no flapping hinges were provided.

The rotors were shaft driven in the helicopter mode by a hydraulic motor and pump arrangement through a roller chain transmission. Rotor speed was controlled by varying the hydraulic pressure at the pump. Rotor cyclic and collective pitch were accomplished through a swash-plate system, the upper part of which was connected to each blade by rigid links. Two different types of swash plate were investigated. The type used for most of the testing had a wave built into it so that it provided 2.5° of second-harmonic cyclic pitch A_2 during each revolution. The other swash plate was of the conventional helicopter type. All of the helicopter data included herein were obtained with the "second-harmonic" swash plate installed. The range of cyclic pitch angle available with either swash plate was from -16° to 16° and the range of collective pitch angle was from -11° to 21.5°.

The model was mounted on a pedestal that was fixed to the ground plane so that the rotor/wing was located approximately 13 feet (3.96 meters) above the ground plane. A six-component strain-gage balance was attached between the top of the pedestal and the model, as shown in figure 6, so that it rotated with the model in the longitudinal plane. The angle of attack of the model was varied by an electric actuator through an available range from about -15° to 20°.

Instrumentation

The forces and moments on the model were sensed by the six-component strain-gage balance. The model angle of attack and rotor control positions were sensed by potentiometers, and the rotor speed was measured by a tachometer.

The output signals from the angle-of-attack, control-position, and rotor-speed sensors were fed to an operator's console which provided visual indication of the model operating conditions and included provisions for varying these conditions. The signals provided at the control console along with the outputs from the balance and a magnetic azimuth position pickup were recorded on an oscillograph. Also, the signals from the balance, the angle-of-attack sensor, and the tunnel static-pressure sensor were electrically fed into a digital readout and tape-recording system. Other pertinent quantities

such as rotor speed, control positions, air density, and hydraulic pressure differential across the balance were manually fed into the digital tape system.

TESTS

All data presented for this investigation were obtained with the horizontal tail removed and the second-harmonic swash plate installed.

Helicopter Mode

The three rotor/wing configurations were investigated in the helicopter mode in hover and in forward flight at tip-speed ratios up to 0.35.

Hovering data were obtained at a rotor speed of 600 revolutions per minute, an angle of attack of 0°, and a cyclic pitch angle of 0° through a range of collective pitch angle from 0° to 20°. Also while in hover, the collective pitch angle was set at a selected value, and the longitudinal and lateral control power available from cyclic-pitch inputs were measured.

Forward flight data were obtained at a rotor speed of 600 revolutions per minute at several free-stream velocities. At each tip-speed ratio, data were obtained for various combinations of angles of attack and collective pitch with the rotor pitching and rolling moments trimmed by cyclic control. Also, at each tip-speed ratio, a combination of angles of attack and collective pitch was selected, and one component of cyclic pitch (A_1 or B_1) was set to trim either the pitching or rolling moments and the other was varied to obtain control data. Then the procedure was reversed and control data for the other axis were obtained.

Airplane Mode

Data for the airplane mode were obtained for the three rotor/wing configurations where the lifting surface was stopped and faired into the fuselage. Configuration 2 was also investigated in the airplane mode with the fairings removed. Forces and moments were measured for a range of angle of attack. The Reynolds number for these tests was 0.58×10^6 per foot (1.9×10^6 per meter).

CORRECTIONS

The data have been corrected for deadweight tares. The forces and moments by which the data were corrected are shown as functions of angle of attack in figure 7 since they were large relative to the overall measurements. The tare loads given in figure 8 were produced by the pressure differential between the supply and return legs of the

hydraulic drive circuit, which was sensed by the balance. The data have also been corrected for these loads. None of the classical wind-tunnel corrections have been applied to the data because they are believed to be small.

PRESENTATION OF RESULTS

The results of this investigation are presented in two basic groups corresponding to the steady-state flight modes of the rotor/wing – helicopter hovering and forward flight, and fixed-wing flight. The figures are presented as given in the following table:

RESULTS AND DISCUSSION

Helicopter Mode

The hovering characteristics of the three rotor/wing configurations are given in figure 9. For $\theta_0 = 0^\circ$ to 20° in figure 9(a), the thrust coefficients for configurations 2 and 3 are in very close agreement, whereas those for configuration 1 are slightly less. The variation of C_T with C_Q was nearly the same for all three configurations. These results can be attributed to the smaller blade area of configuration 1. The variation of rotor figure of merit with thrust coefficient (fig. 9(b)) indicates that at the normal hovering thrust coefficient ($C_T = 0.008$ for the full-scale aircraft from the data of ref. 1) the differences in figure of merit for the rotor configurations are small. Since these rotors would normally operate near their maximum efficiency, they would all benefit from design modifications which increase the maximum attainable figures of merit since the maximum obtained from the present rotors was less than 0.5.

The aerodynamic and control characteristics for helicopter-mode forward flight given in figures 10, 11, and 12 indicate similar trends for each of the three configurations throughout the range of tip-speed ratios. The values of lift, drag, and cyclic control required for trim were in close agreement. At the lower tip-speed ratios, however, the torque coefficients for configuration 1 at the highest collective-pitch-angle settings were appreciably lower than those for the other configurations. Nearly all available B_1 cyclic control was required to trim the model rolling moments at combinations of high tip-speed ratio and high collective-pitch-angle settings. The A_1 control required to trim the pitching moments at the same conditions was generally less than one-half of that available. The variation of cyclic control power with tip-speed ratio (fig. 13) shows similar control characteristics for the three configurations. The differences shown for positive and negative control inputs are the result of the asymmetry of loading around the rotor disk. The curves shown in figure 13 suggest that at tip-speed ratios greater than those of this investigation $(V/\Omega R = 0.35)$, the control power differences resulting from positive and negative inputs may become even larger.

From the foregoing discussion of the hovering and forward-flight results, there appears to be little basis for a clear choice between the three rotor/wing configurations as a "pure" helicopter lift-propulsion system. The hovering results, in particular, suggest that all three configurations would benefit from improved blade cross sections. The provision of blades having lower thickness ratio with perhaps a moderate amount of camber could possibly result in better performance in both hovering and forward flight. Naturally, any modification must be made within the constraints imposed by the fixed-wing cruise requirements.

Airplane Mode

The longitudinal aerodynamic characteristics of the model with each of the rotor/wing configurations in the airplane cruise mode are given in figure 14. The differences between the three configurations were generally small when operating in the helicopter mode, but considerably different results are indicated for fixed-wing conditions. The variation of pitching-moment coefficient with angle of attack (horizontal tail off) shows that configuration 3 has considerably less static instability and lower trim requirements than the other two configurations. On this basis, the required horizontal tail for configuration 3 would incur the lowest trimmed drag and, thus, provide for an aircraft with higher cruise efficiency than one using either of the other two rotor/wing configurations. In the normal range of cruise lift coefficients, the addition of fairings to the wing-fuselage juncture of configuration 2 reduced the out-of-trim pitching moment while leaving the static longitudinal stability relatively unchanged. It is believed that the presence of fairings on configurations 1 and 3 would produce similar results.

The important result obtained from this discussion is that configuration 2, which had the highest efficiency as a hovering rotor, was less favorable than configuration 3 when it was flown as a fixed wing. Consequently, extreme care must be exercised in designing a composite lifting surface to obtain both an efficient rotor and an efficient wing. The extent to which design trade-offs between rotor and wing efficiencies can be made will naturally depend upon the aircraft mission.

CONCLUSIONS

A wind-tunnel investigation of the aerodynamic characteristics of a composite-lift aircraft model in the helicopter and airplane flight modes indicates the following conclusions:

1. There are no significant differences in rotor hovering efficiency between the three rotor/wing configurations at the normal hovering thrust coefficient. The maximum figure of merit attained was less than 0.5.

2. The aerodynamic and control characteristics of the model operating in the helicopter cruise mode exhibit only small differences between the three configurations. Data from all three configurations indicate that roll control may become a problem at combinations of high-speed and high collective pitch settings.

3. Both the hovering and forward flight results from the helicopter mode investigation indicate the need for improvement of the rotor blades. It is believed that considerable improvement could be made by modifying the relatively thick, biconvex blade cross sections used on this model.

4. The results of the airplane cruise mode investigation indicate the need for extreme care in the design of composite lifting surfaces in order to obtain both an efficient rotor and an efficient fixed wing.

Langley Research Center,
National Aeronautics and Space Administration,
Langley Station, Hampton, Va., March 20, 1969,
721-01-00-36-23.

REFERENCES

1. Huston, Robert J.; and Shivers, James P.: A Wind-Tunnel and Analytical Study of the Conversion From Wing Lift to Rotor Lift on a Composite-Lift VTOL Aircraft. NASA TN D-5256, 1969.

2. Mechtly, E. A.: The International System of Units – Physical Constants and Conversion Factors. NASA SP-7012, 1964.

TABLE I.- MODEL DETAILS

	Configuration 1	Configuration 2	Configuration 3
Rotor:			
Rotor radius, ft (m)	3.58 (1.09)	3.58 (1.09)	3.58 (1.09)
Hub area, ft^2 (m^2)	12.23 (1.14)	9.90 (0.92)	7.73 (0.72)
Blade area (1 blade, outboard of 0.55 radius), ft^2 (m^2)	0.82 (0.08)	1.04 (0.10)	1.04 (0.10)
Total planform area, ft^2 (m^2)	14.69 (1.36)	13.02 (1.21)	10.85 (1.01)
Blade chord –			
Root (at 0.55 radius), ft (m)	0.56 (0.17)	0.89 (0.27)	0.89 (0.27)
Tip, ft (m)	0.56 (0.17)	0.56 (0.17)	0.56 (0.17)
Radius of curvature between blades in planform view, ft (m)	4.04 (1.23)	∞	-4.17 (-1.27)
Blade cross section	15 percent thick elliptical	15 percent thick elliptical	15 percent thick elliptical
Wing:			
Wing span, ft (m)	6.42 (1.96)	6.42 (1.96)	6.42 (1.96)
Average chord, ft (m)	2.16 (0.66)	1.87 (0.57)	1.53 (0.47)
Aspect ratio	2.97	3.44	4.19
Wing cross section	15 percent thick elliptical	15 percent thick elliptical	15 percent thick elliptical

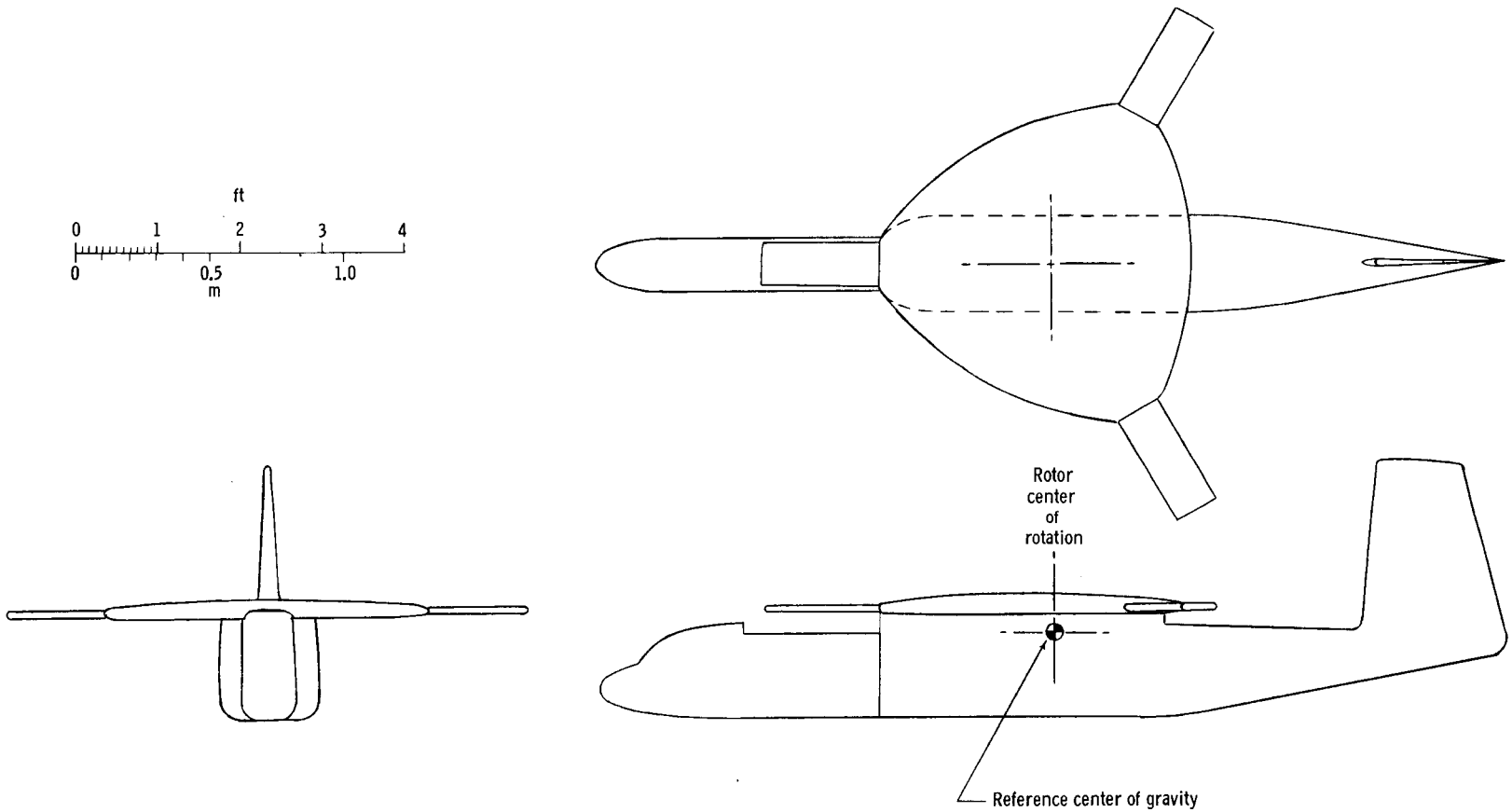

(a) Three-view drawings of model (rotor configuration 1).

Figure 1.- Rotor/wing model.

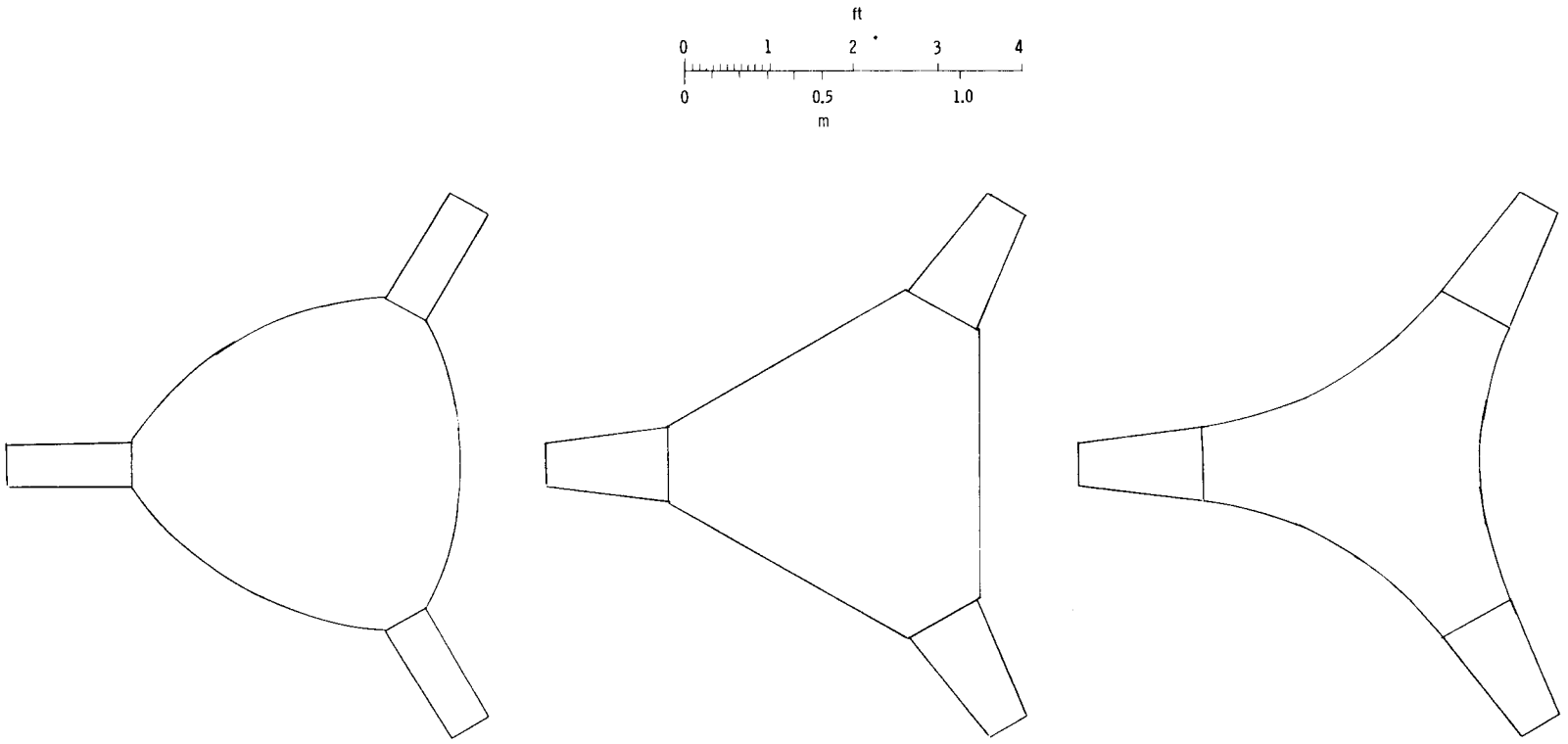

(b) Plan views of rotor configurations.

Figure 1.- Concluded.

Figure 2.- Model installed in the Langley full-scale tunnel.

L-66-7293

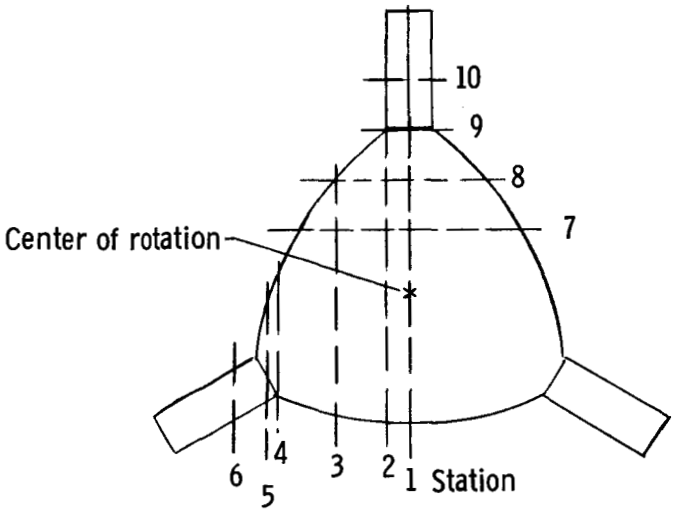

Station location from center of rotation, radial or lateral distance, $\psi = 60°$

Sta.	Inches	Centimeters
1	0	0
2	5.18	13.16
3	12.82	32.56
4	17.95	45.59
5	22.20	56.39
6	29.56	75.08
7	9.83	24.97
8	17.20	43.69
9	24.57	62.41
10	30.00	76.20

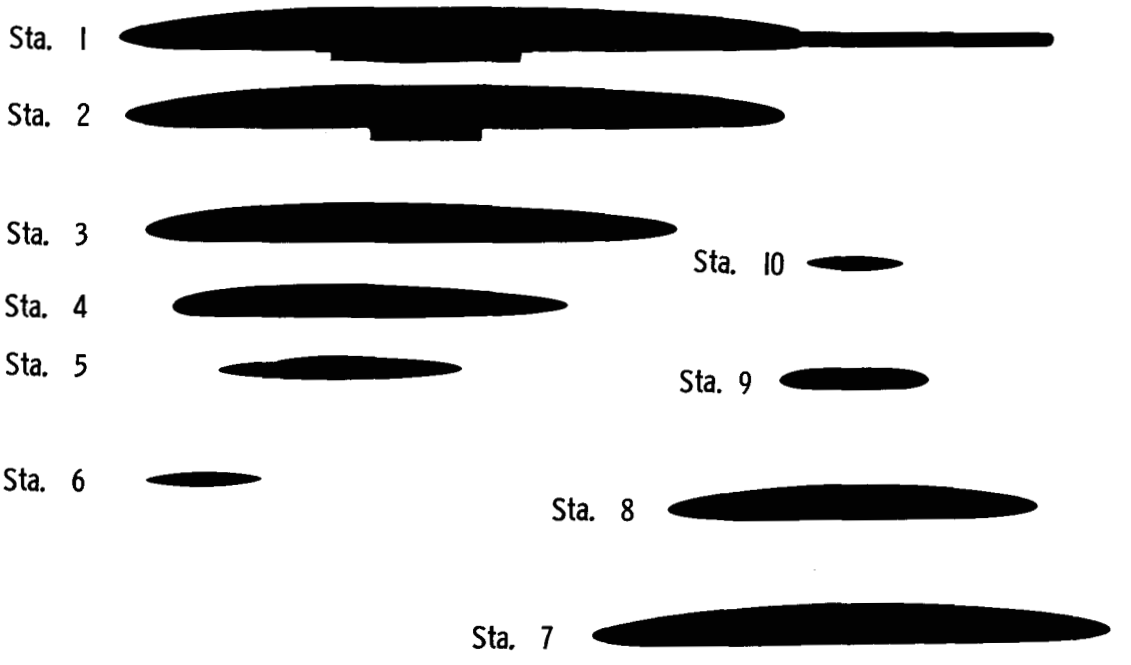

Figure 3.- Section details of rotor/wing configuration 1.

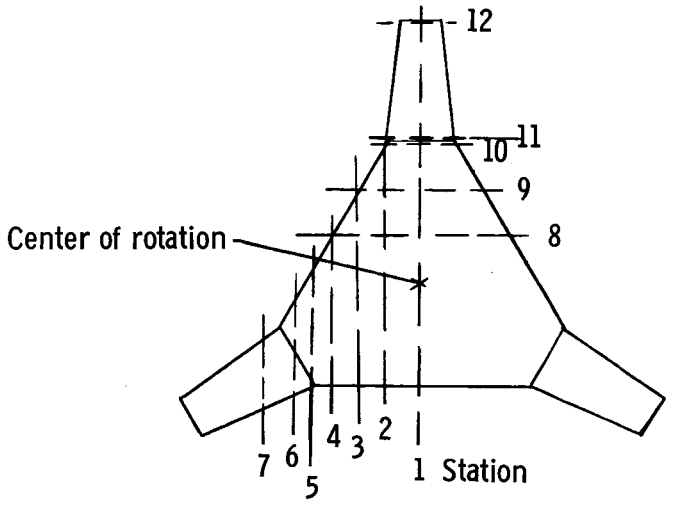

Station location from center of rotation, radial or lateral distance, $\psi = 60°$

Sta.	Inches	Centimeters
1	0	0
2	6.21	15.77
3	11.00	27.96
4	15.50	39.37
5	19.50	49.53
6	22.00	55.88
7	26.75	67.95
8	8.70	22.10
9	16.53	41.99
10	24.36	61.87
11	26.36	66.95
12	41.95 (1 from tip)	106.54 (2.54 from tip)

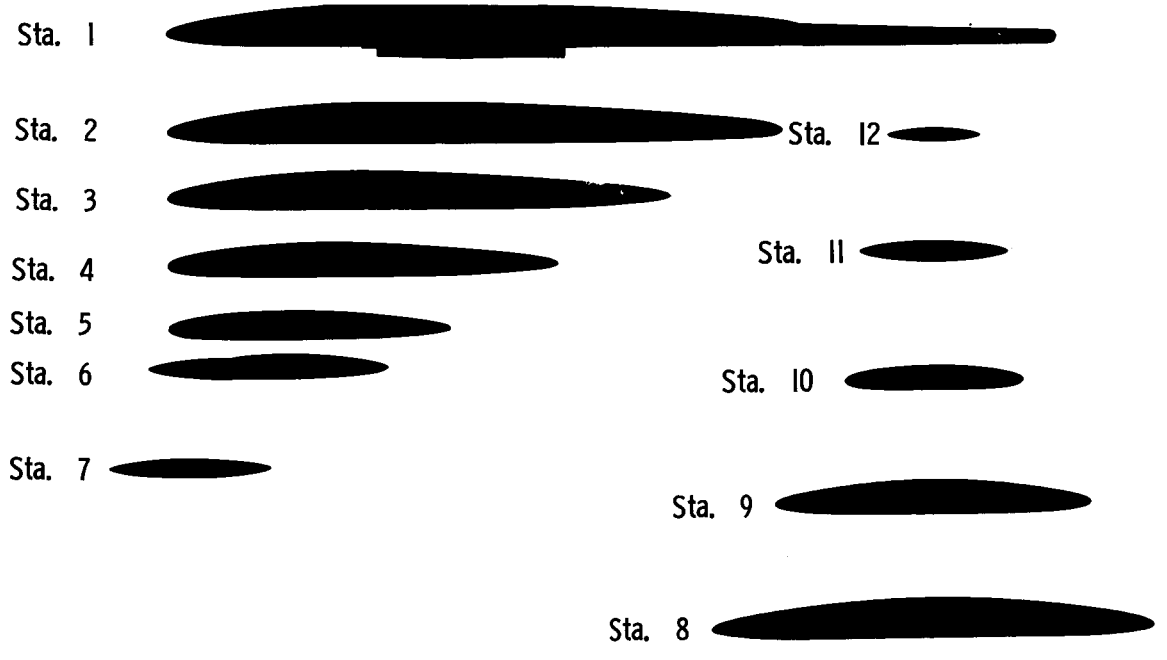

Figure 4.- Section details of rotor/wing configuration 2.

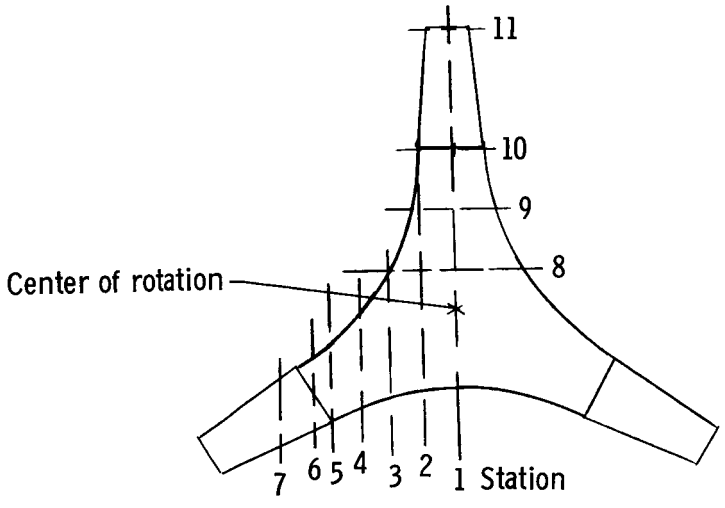

Station location from center of rotation, radial or lateral distance, $\psi = 60°$

Sta.	Inches	Centimeters
1	0	0
2	5.43	13.79
3	11.68	29.67
4	15.68	39.83
5	19.50	49.53
6	22.00	55.88
7	26.75	67.95
8	6.68	16.97
9	15.50	39.37
10	24.56	62.38
11	41.95 (1 from tip)	106.54 (2.54 from tip)

Figure 5.- Section details of rotor/wing configuration 3.

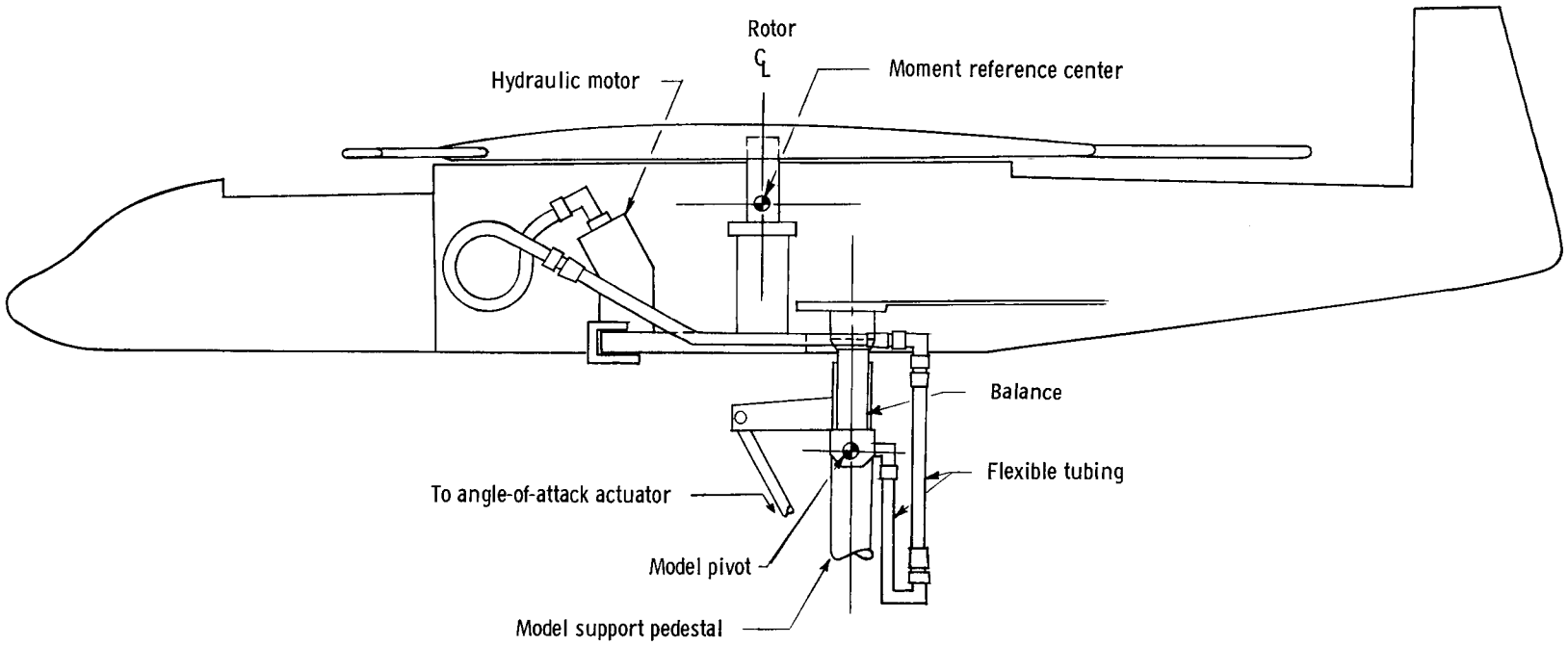

Figure 6.- Model mounting system, balance installation, and hydraulic drive motor arrangement.

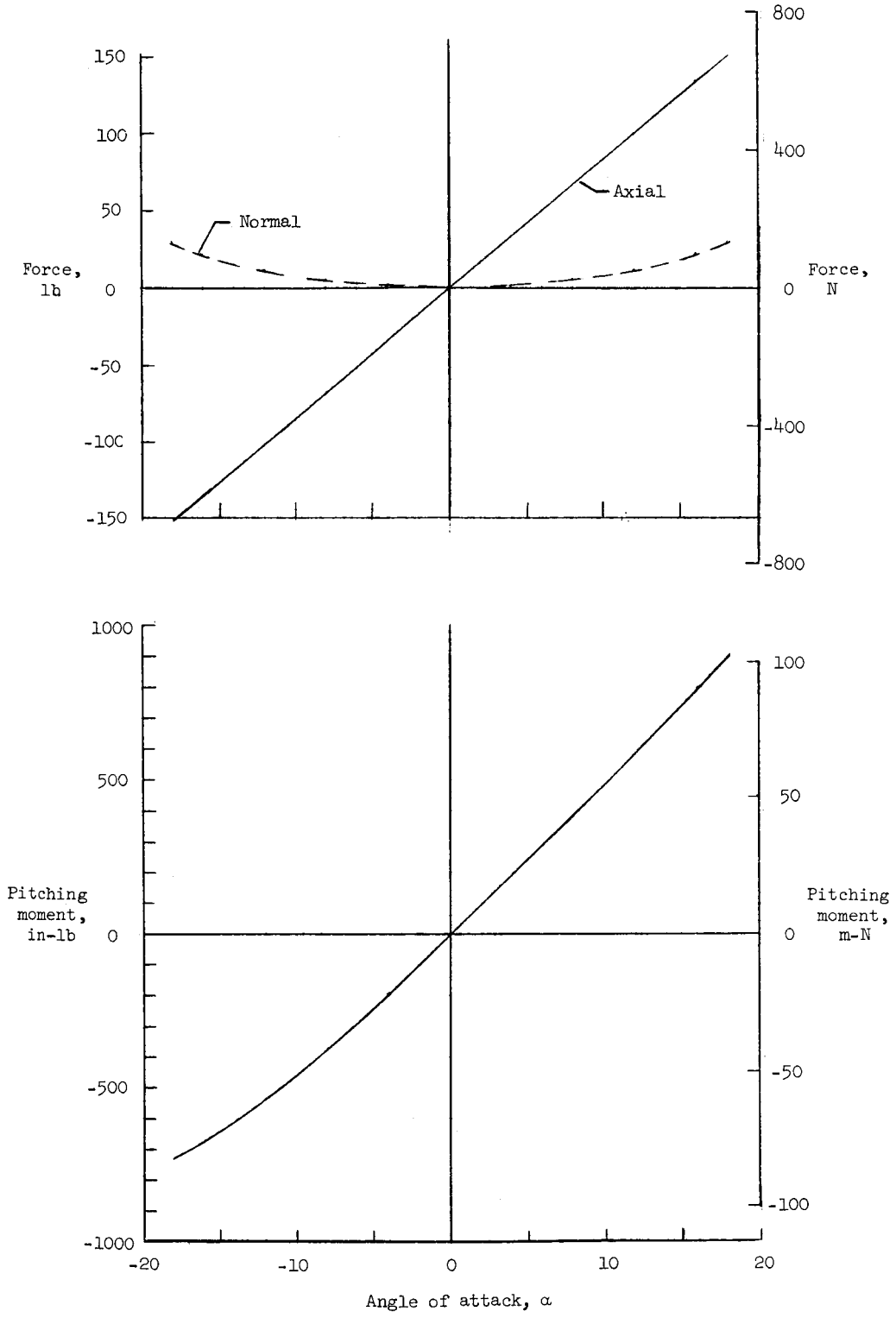

Figure 7.- Angle-of-attack tares.

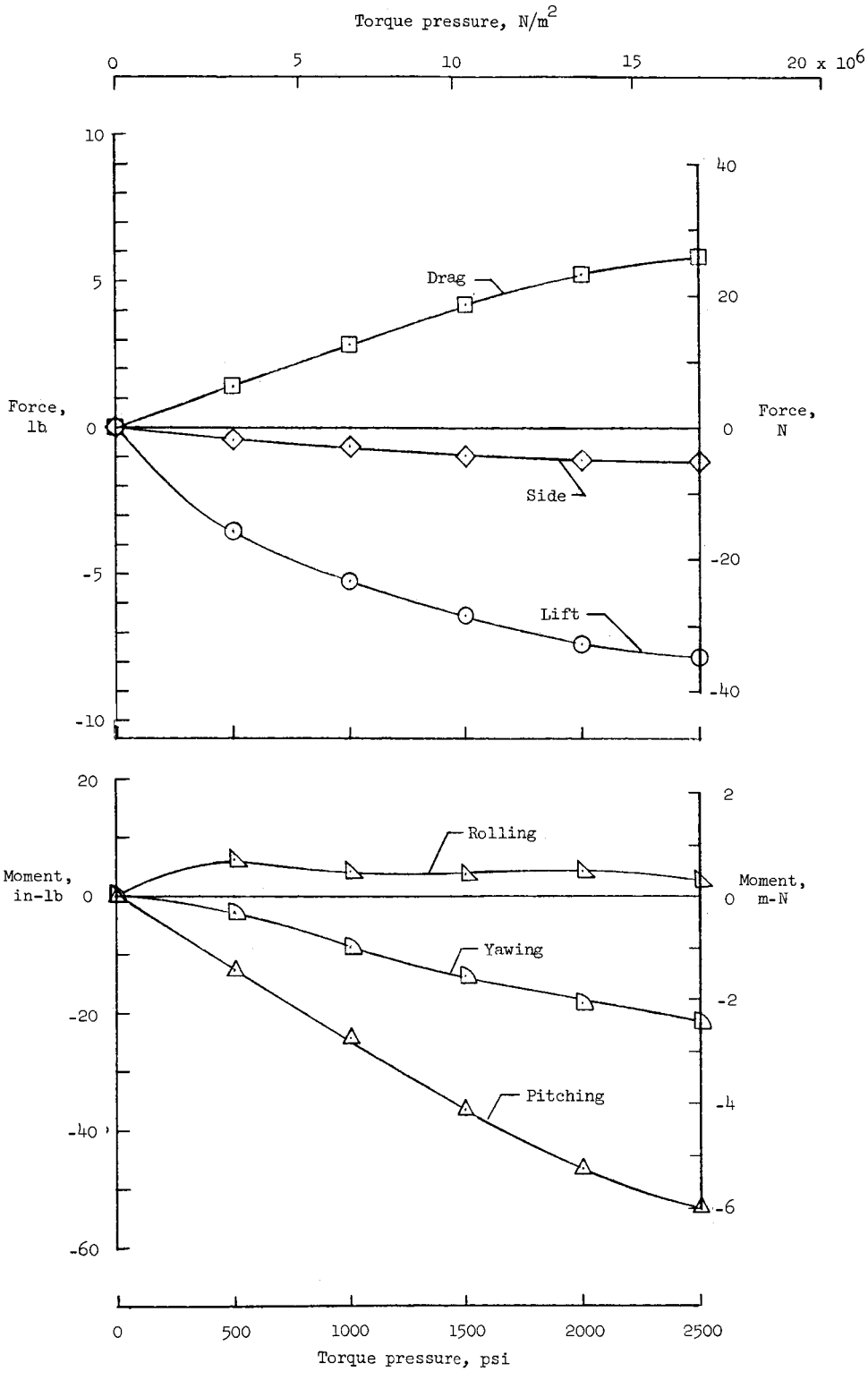

Figure 8.- Torque-pressure tares removed from measured forces and moments.

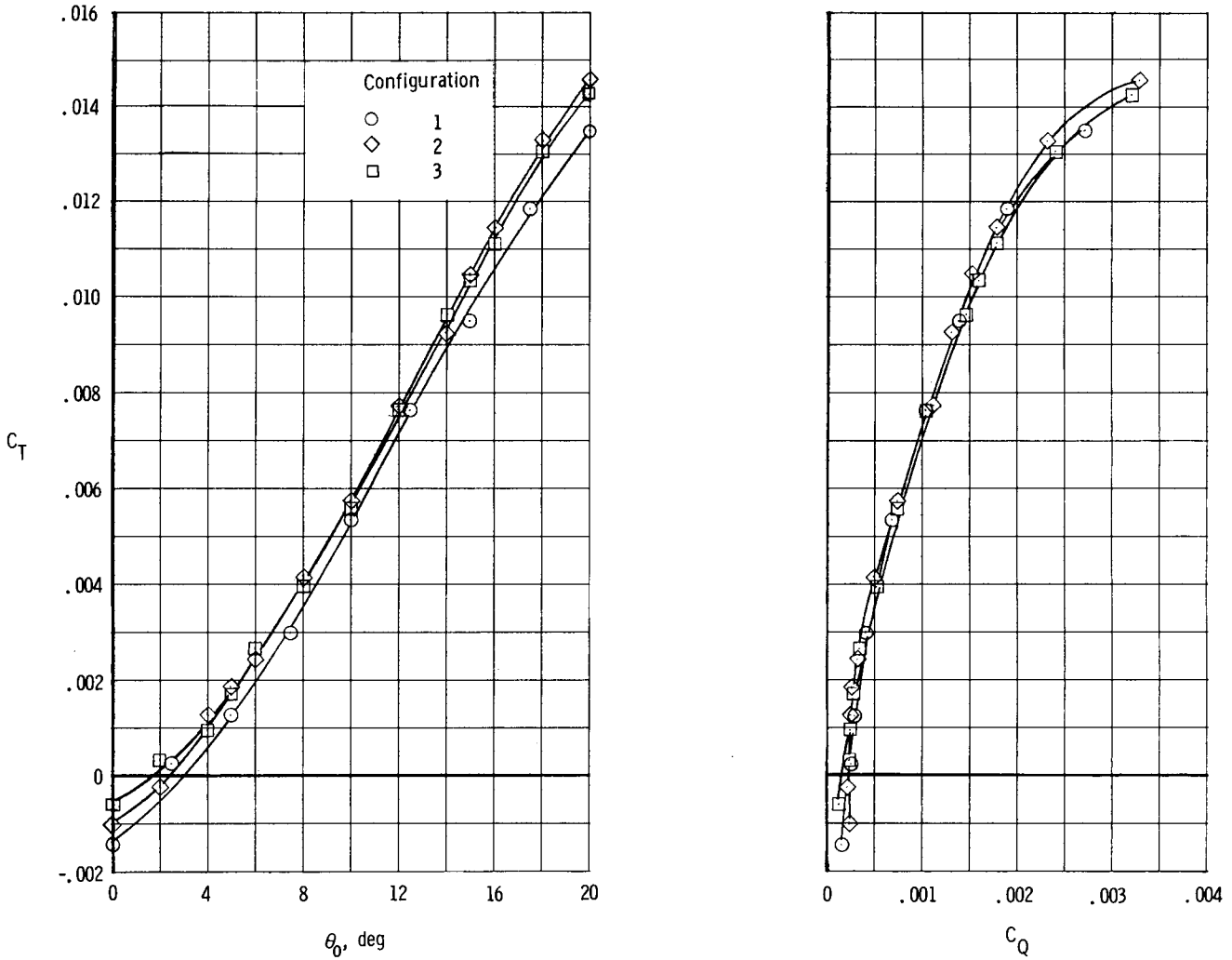

(a) Variation of thrust coefficient with collective pitch angle and torque coefficient.

Figure 9.- Hovering characteristics of rotor/wing configurations.

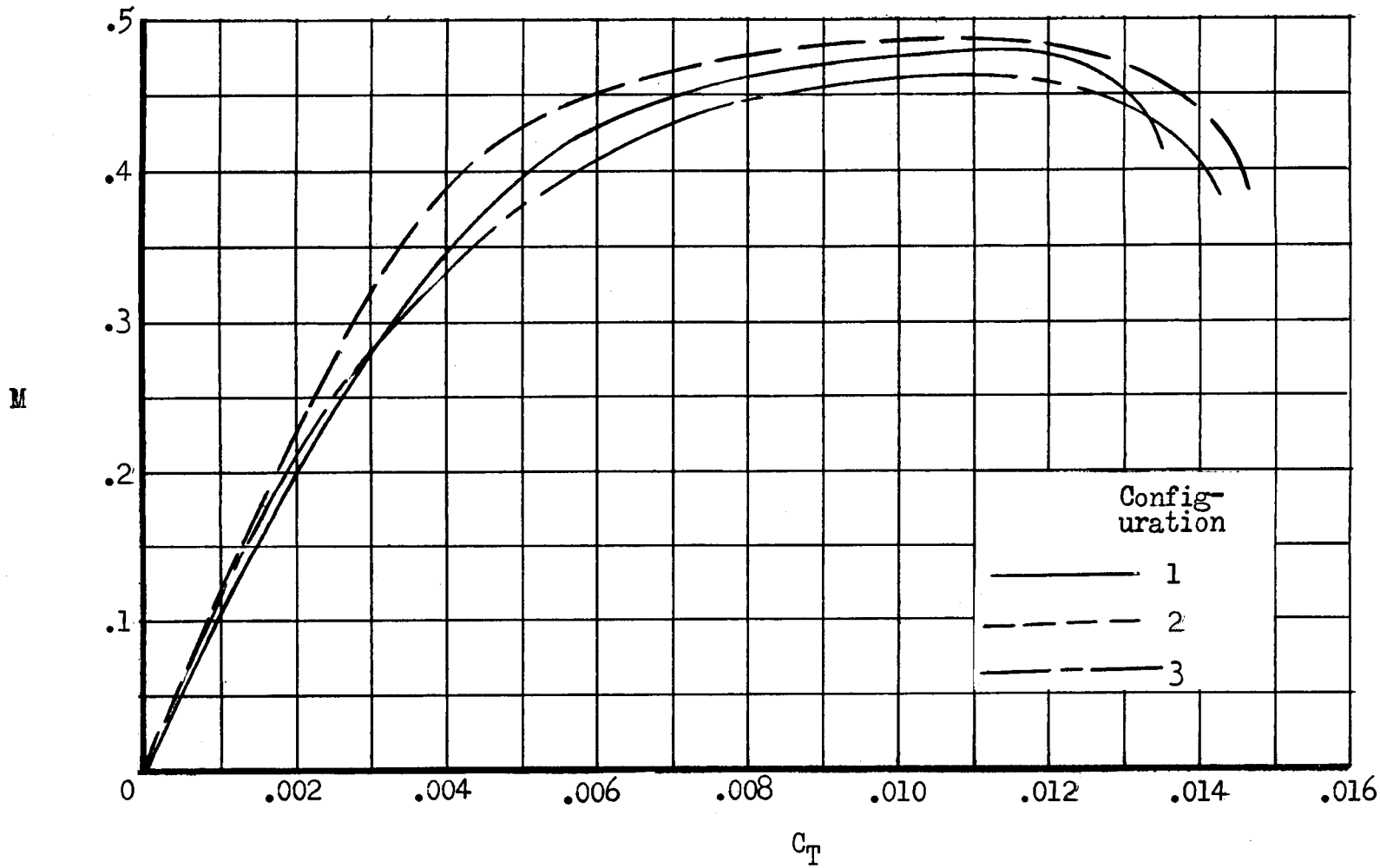

(b) Variation of rotor figure of merit with thrust coefficient.

Figure 9.- Concluded.

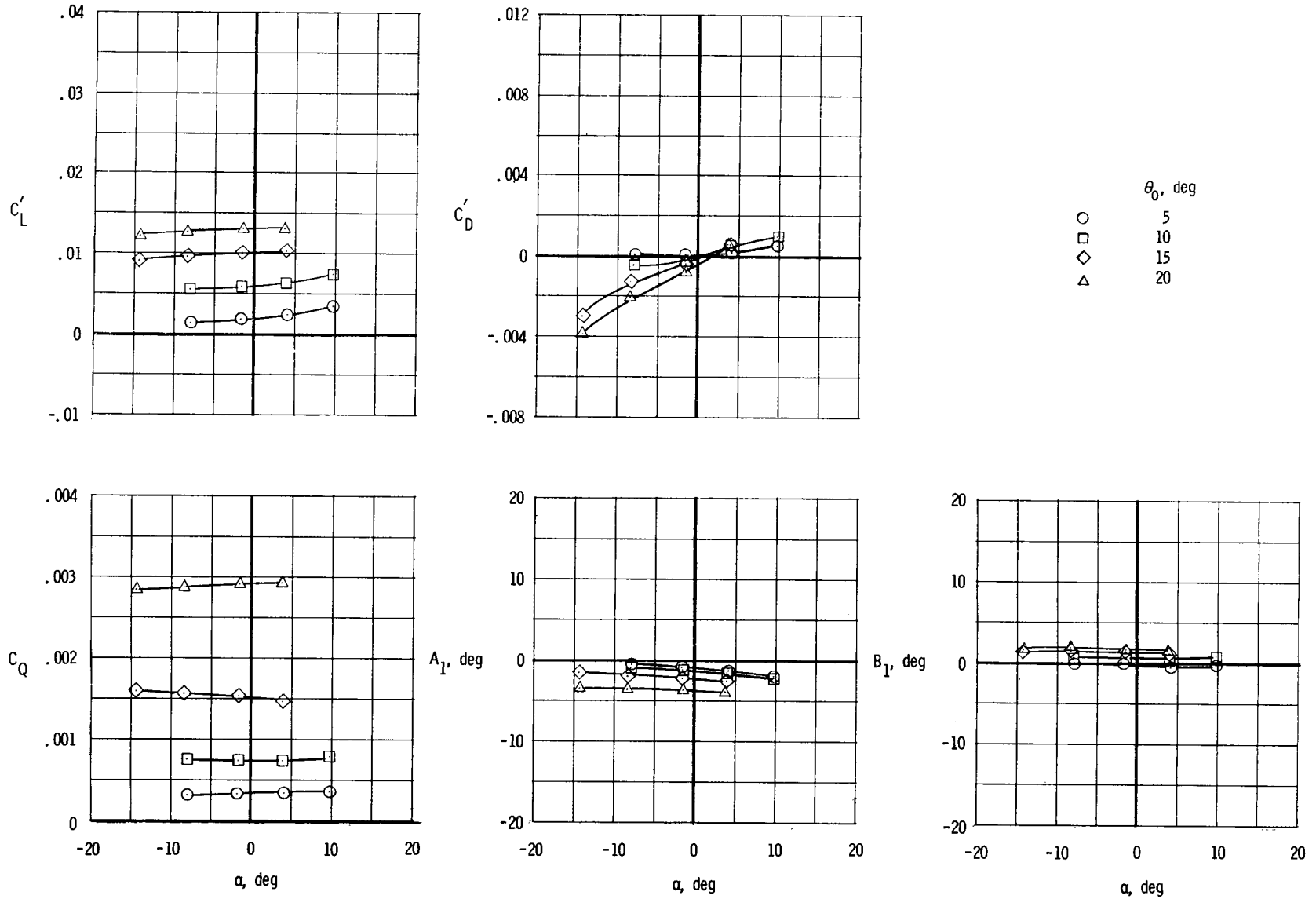

(a) $V/\Omega R = 0.05$.

Figure 10.- Aerodynamic and control characteristics of configuration 1 in helicopter mode. $C_m' = C_l' = 0$.

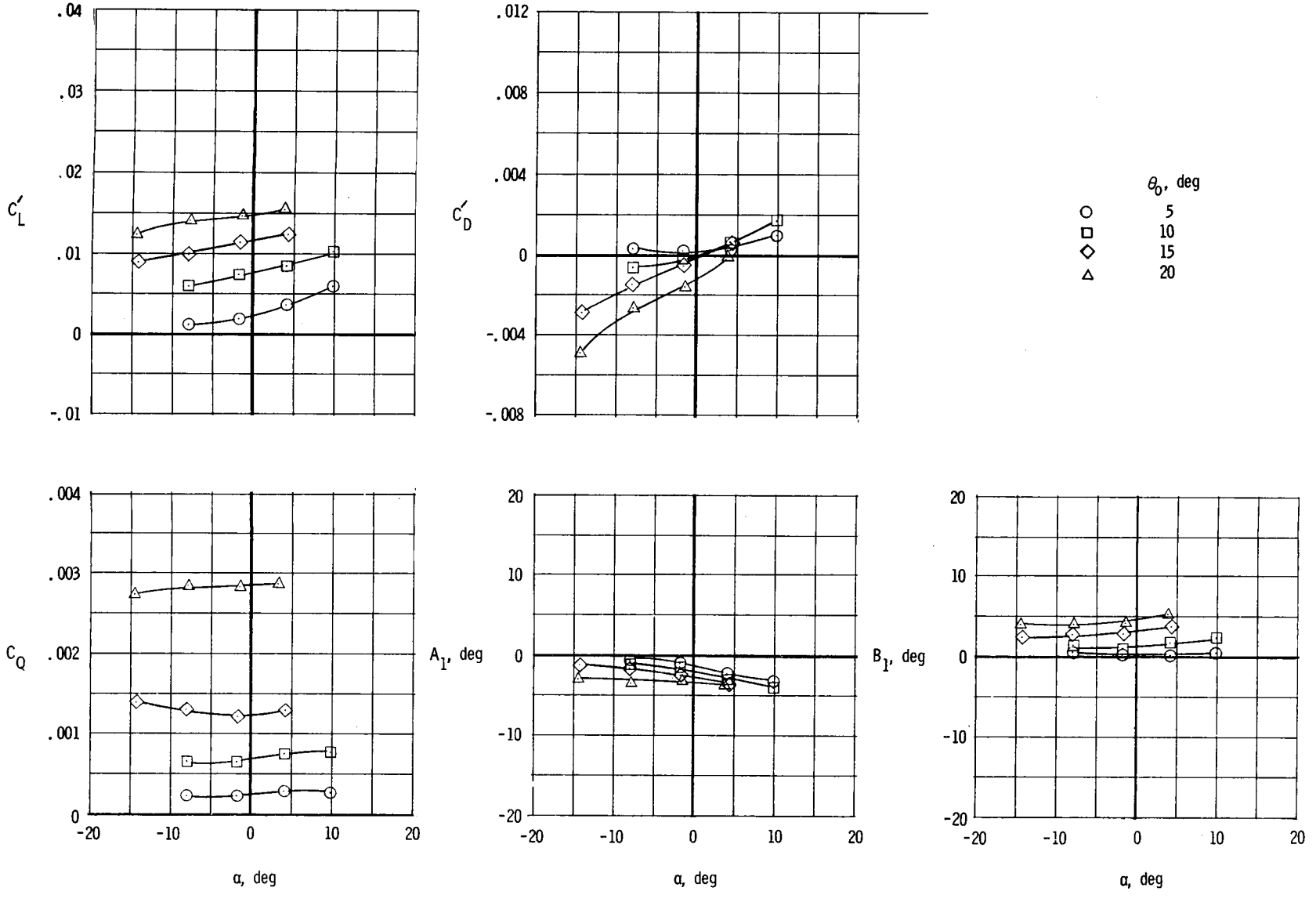

(b) $V/\Omega R = 0.10$.

Figure 10.- Continued.

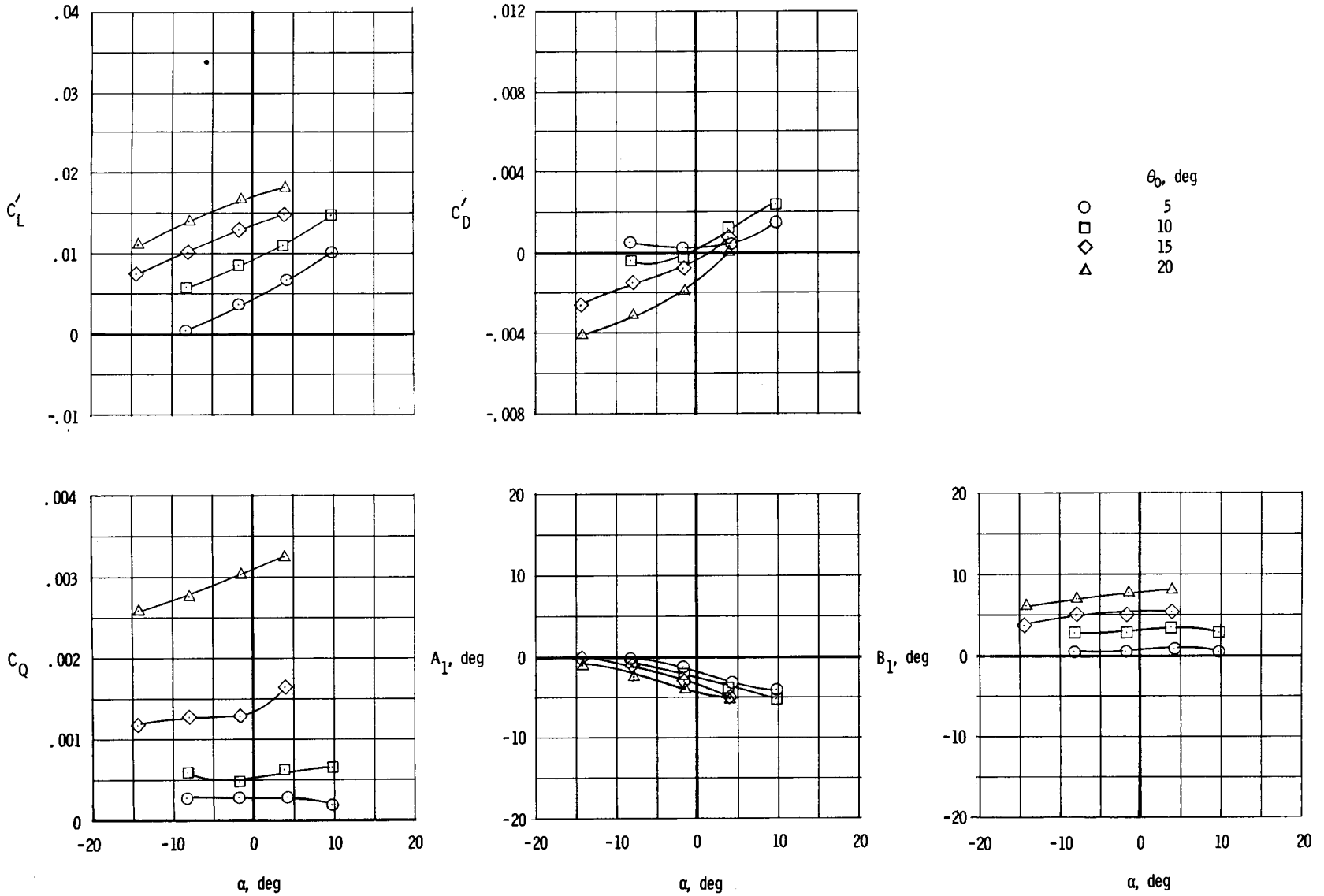

(c) $V/\Omega R = 0.15$.

Figure 10.- Continued.

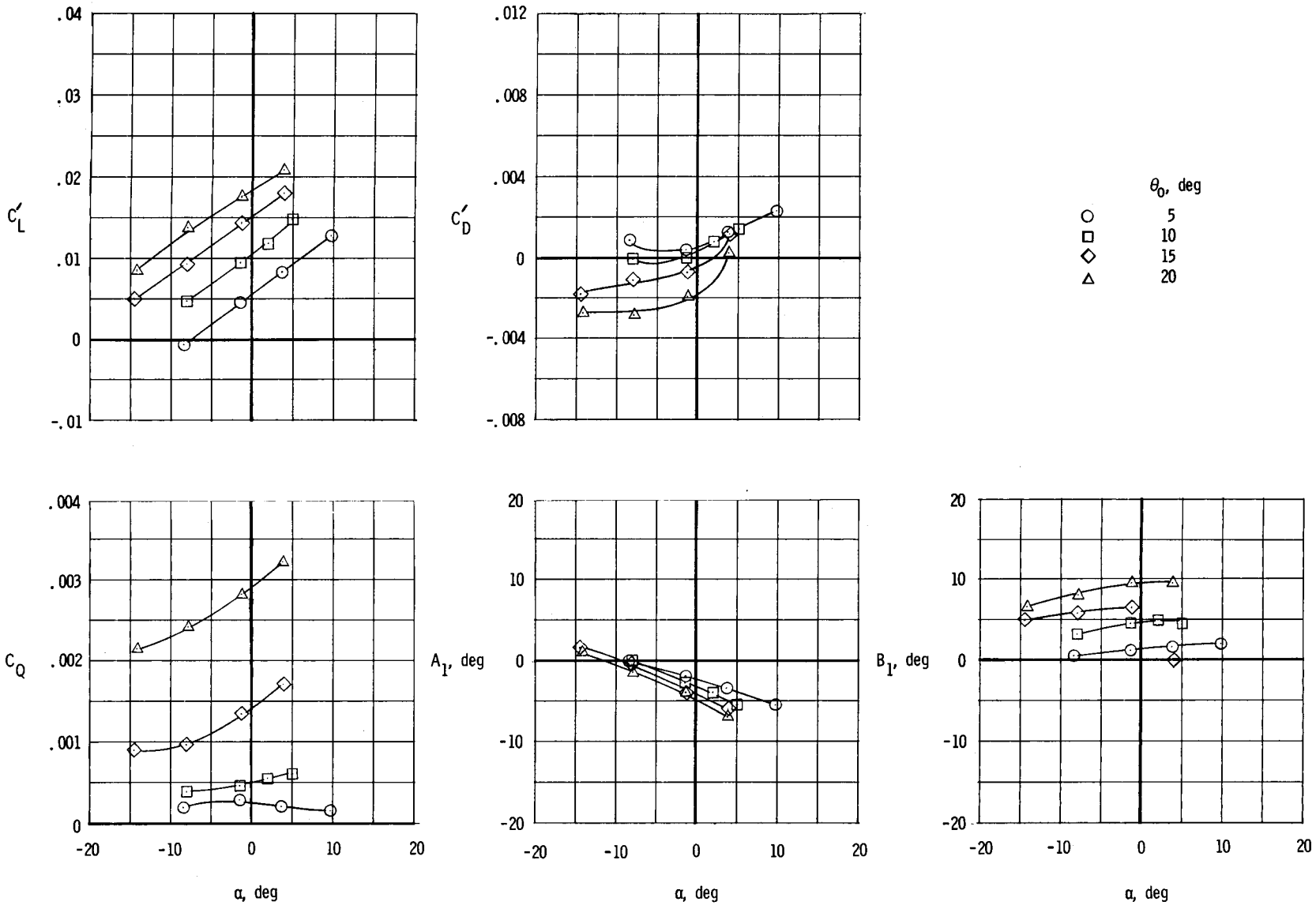

(d) $V/\Omega R = 0.25$.

Figure 10.- Continued.

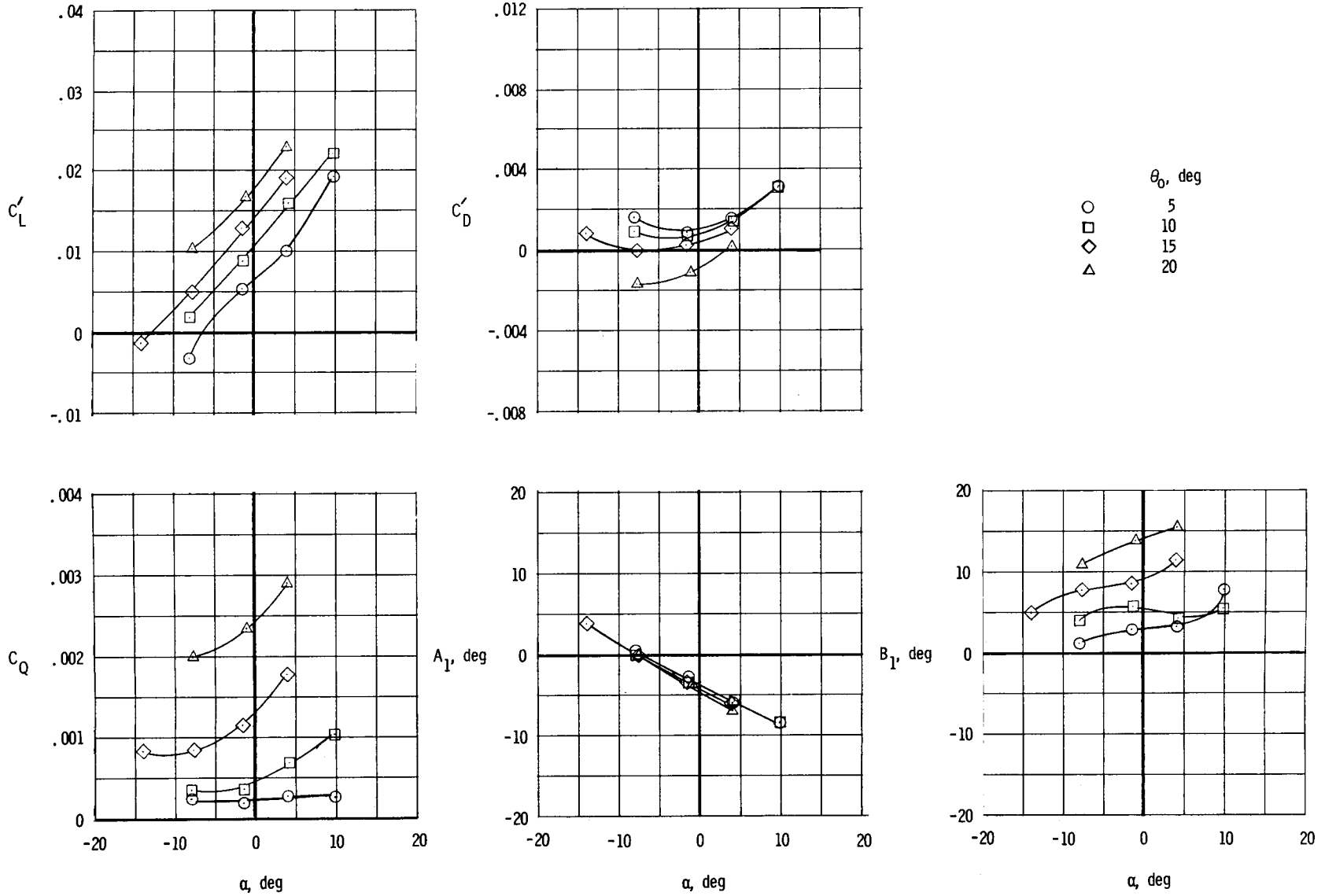

(e) $V/\Omega R = 0.35$.

Figure 10.- Concluded.

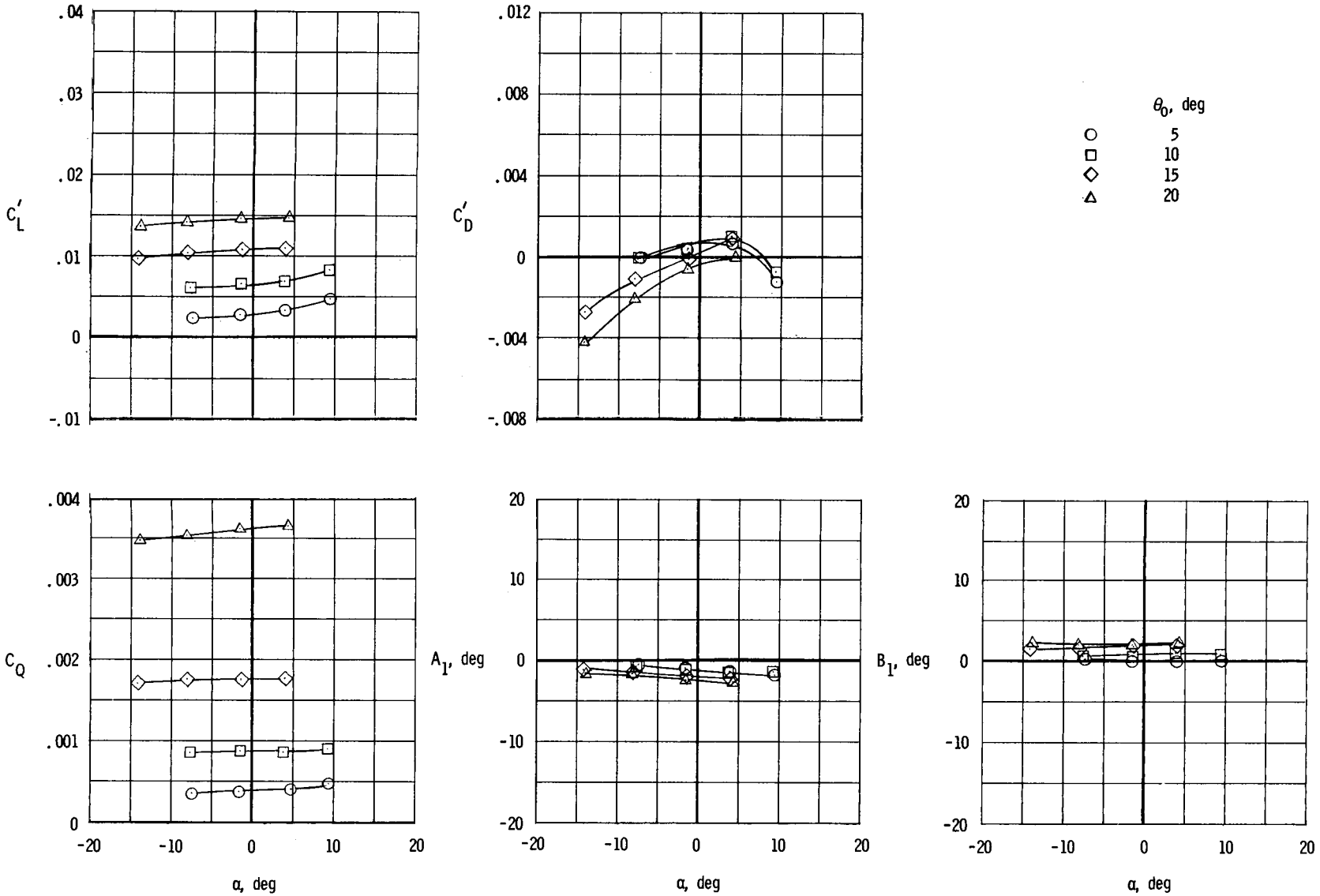

(a) $V/\Omega R = 0.05$.

Figure 11.- Aerodynamic and control characteristics of configuration 2 in helicopter mode. $C'_m = C'_l = 0$.

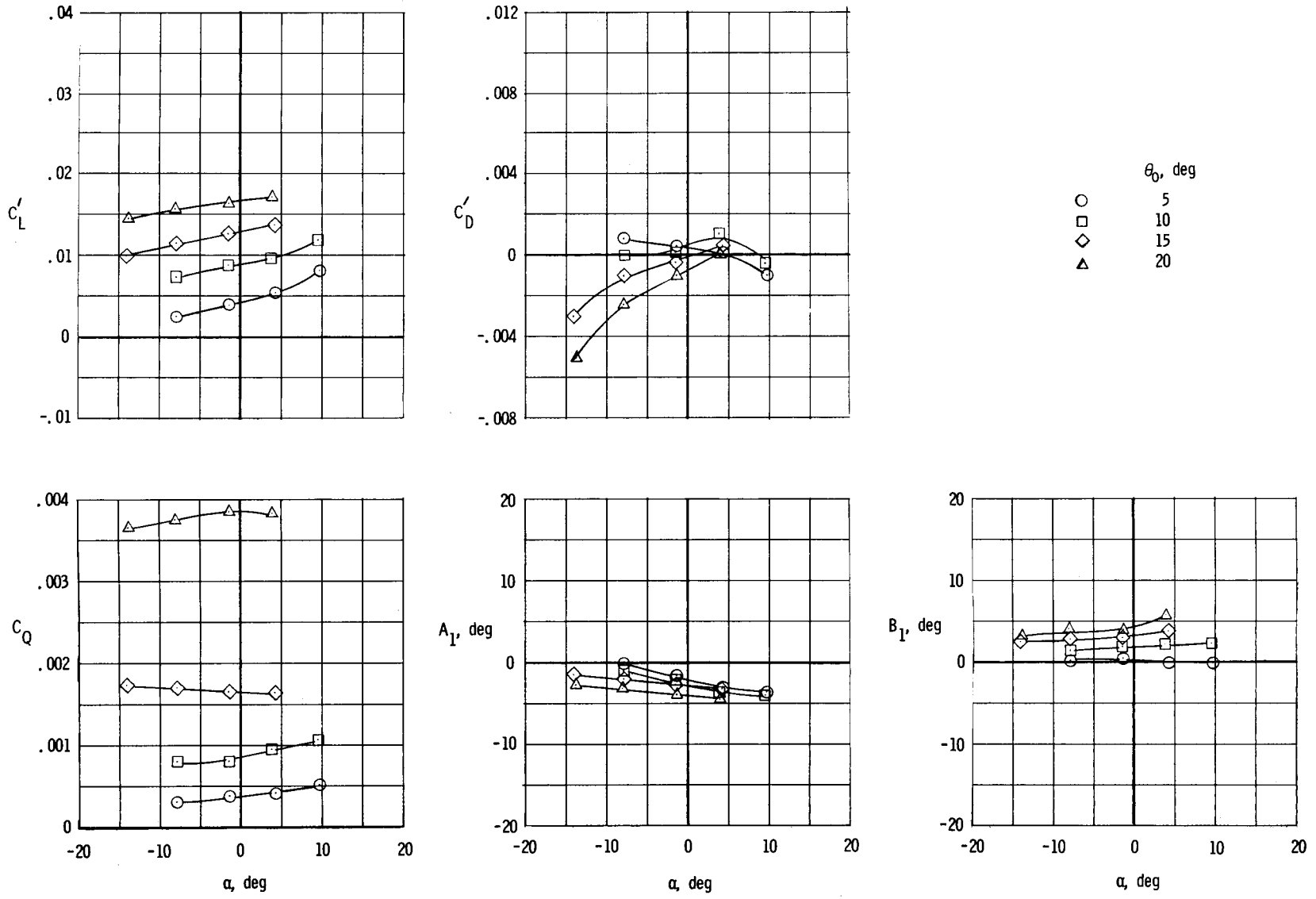

(b) $V/\Omega R = 0.10$.

Figure 11.- Continued.

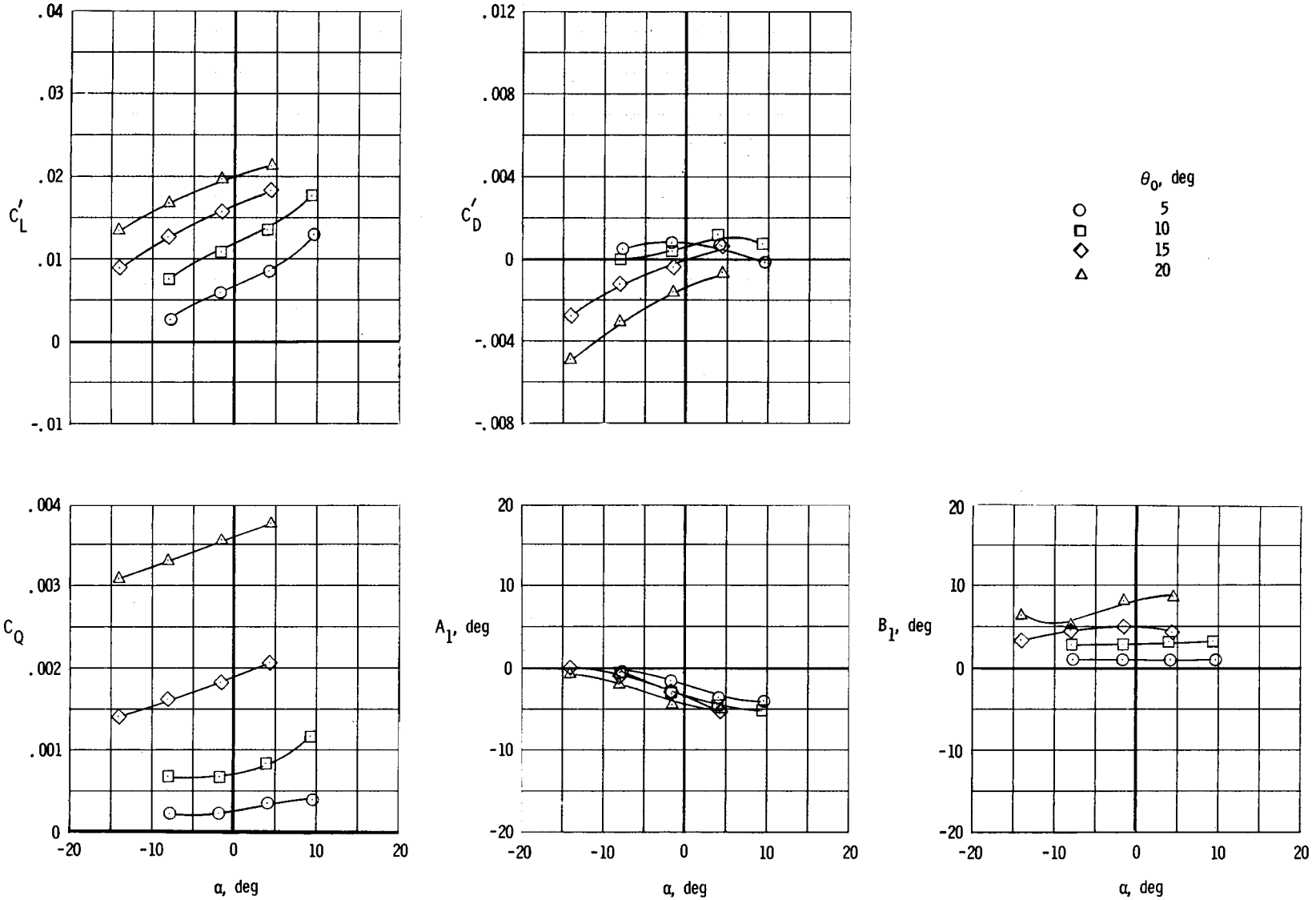

(c) $V/\Omega R = 0.15$.

Figure 11.- Continued.

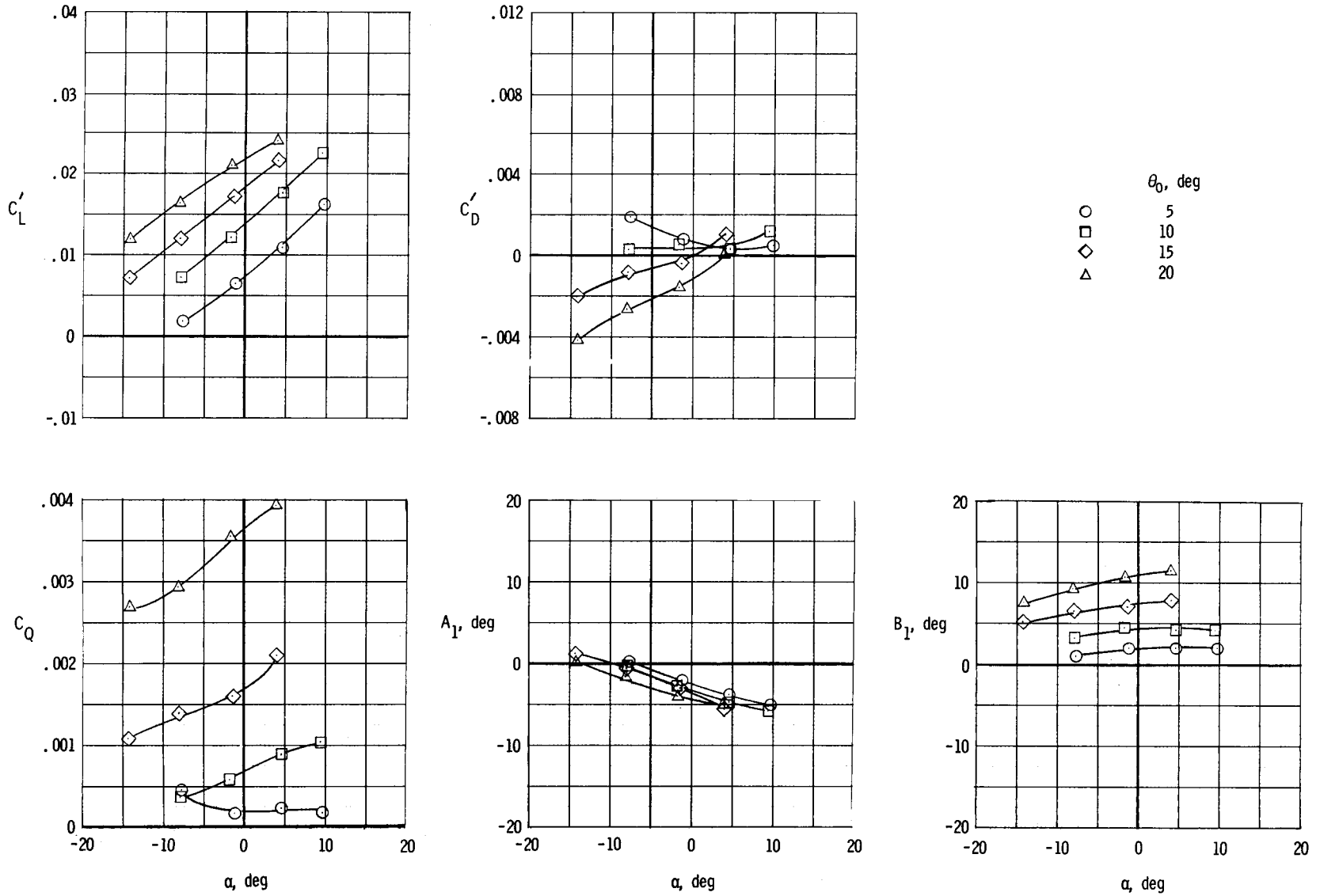

(d) $V/\Omega R = 0.25$.

Figure 11.- Continued.

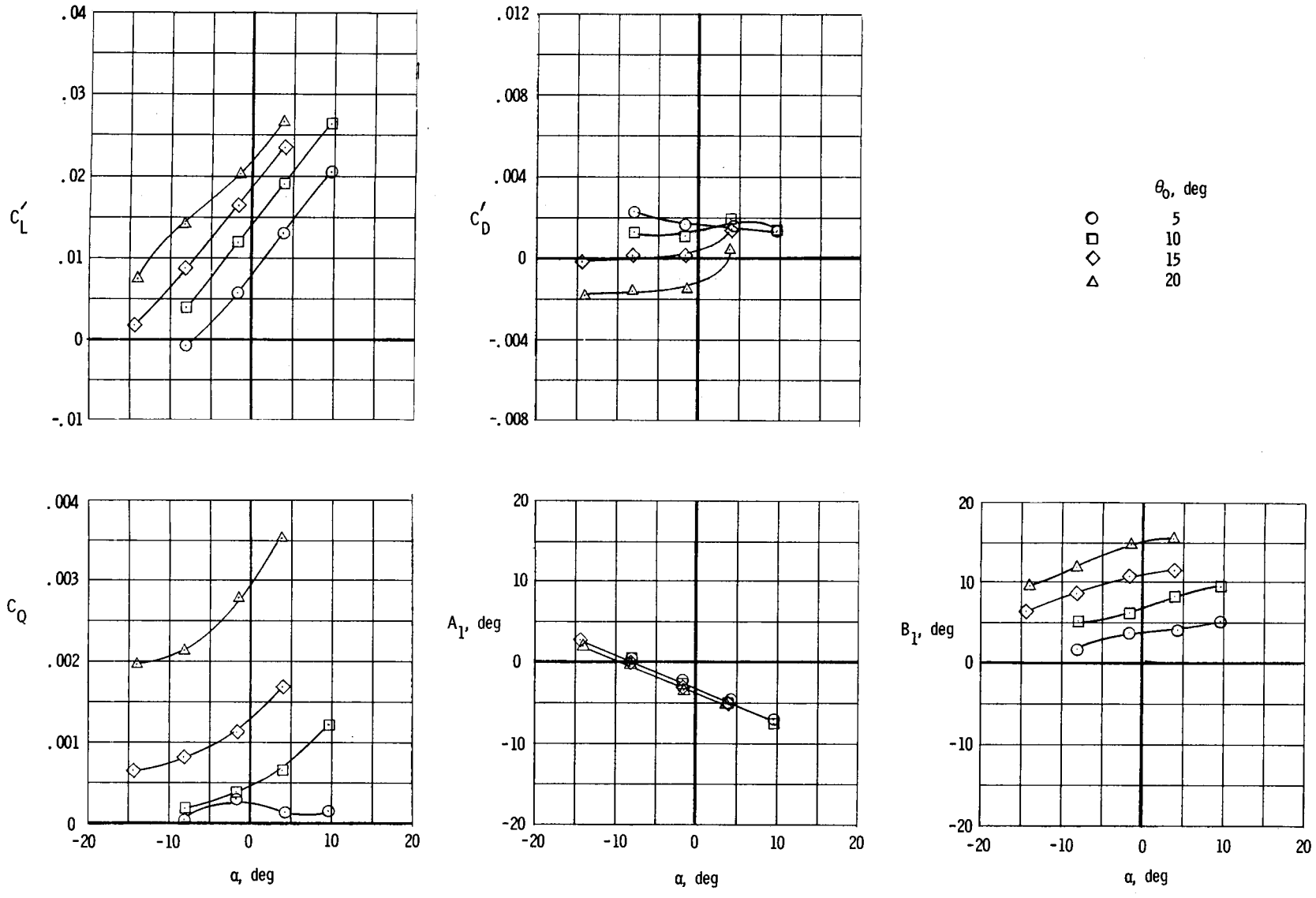

(e) $V/\Omega R = 0.35$.

Figure 11.- Concluded.

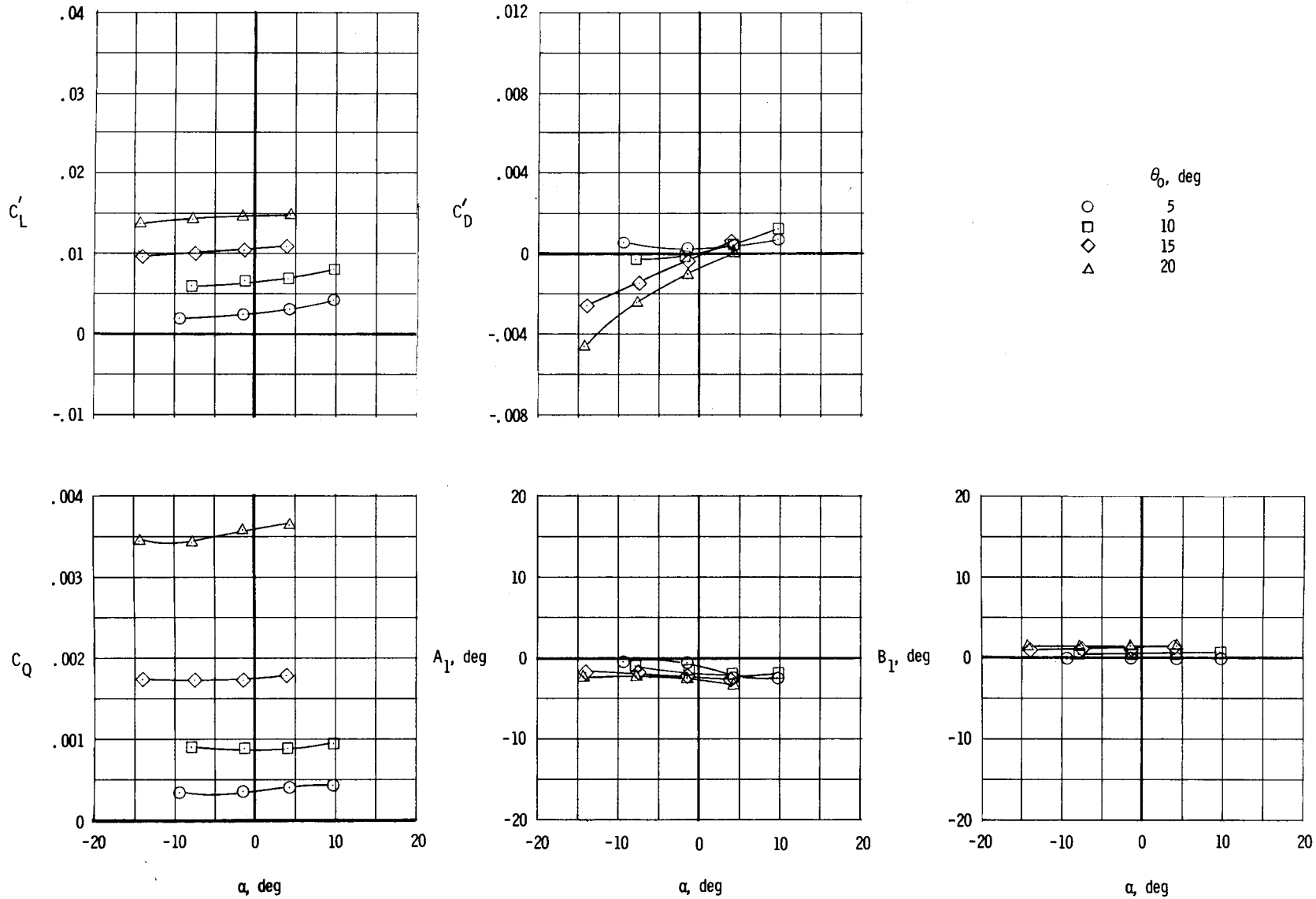

(a) $V/\Omega R = 0.05$.

Figure 12.- Aerodynamic and control characteristics of configuration 3 in helicopter mode. $C_m' = C_l' = 0$.

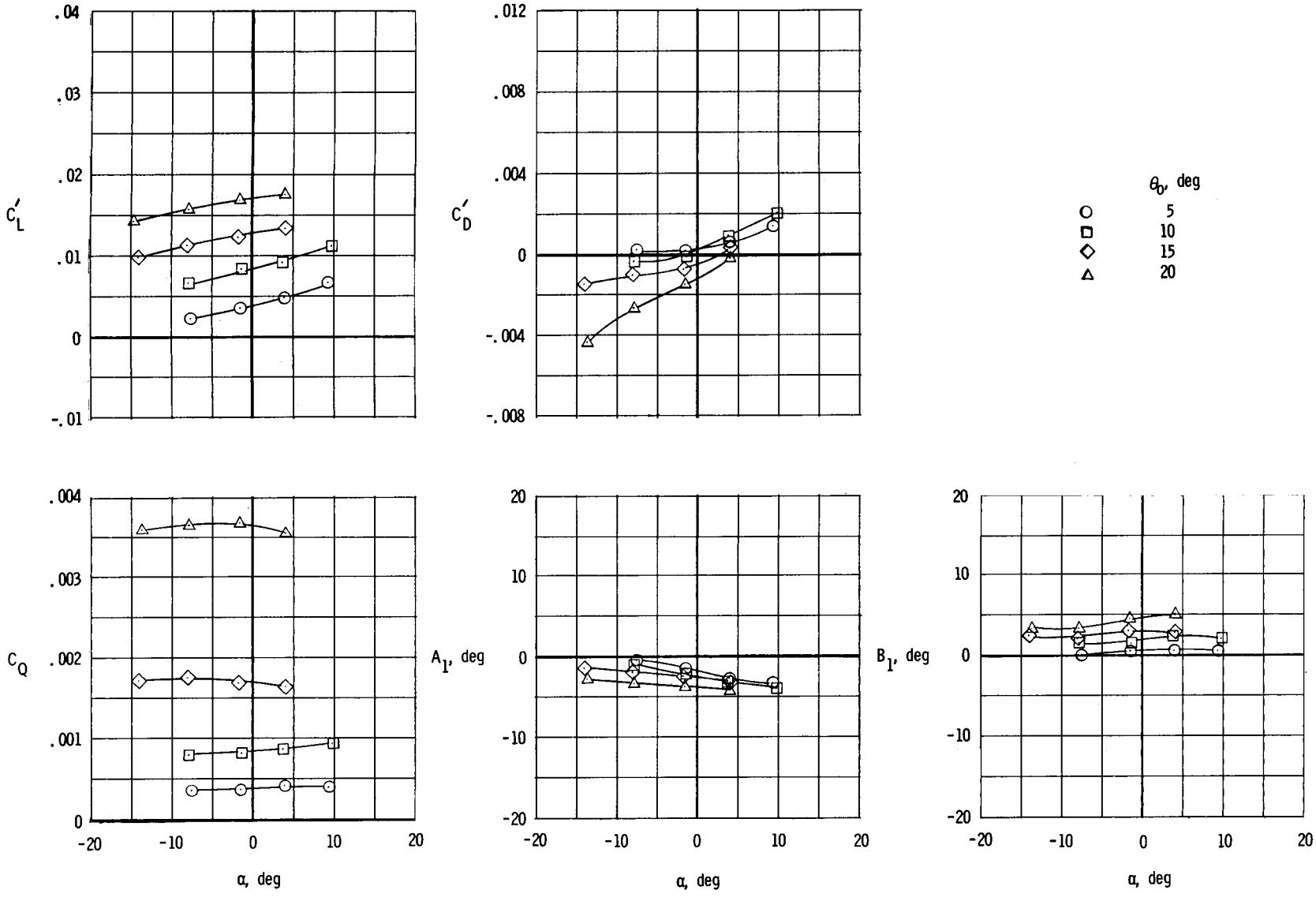

(b) $V/\Omega R = 0.10$.

Figure 12.- Continued.

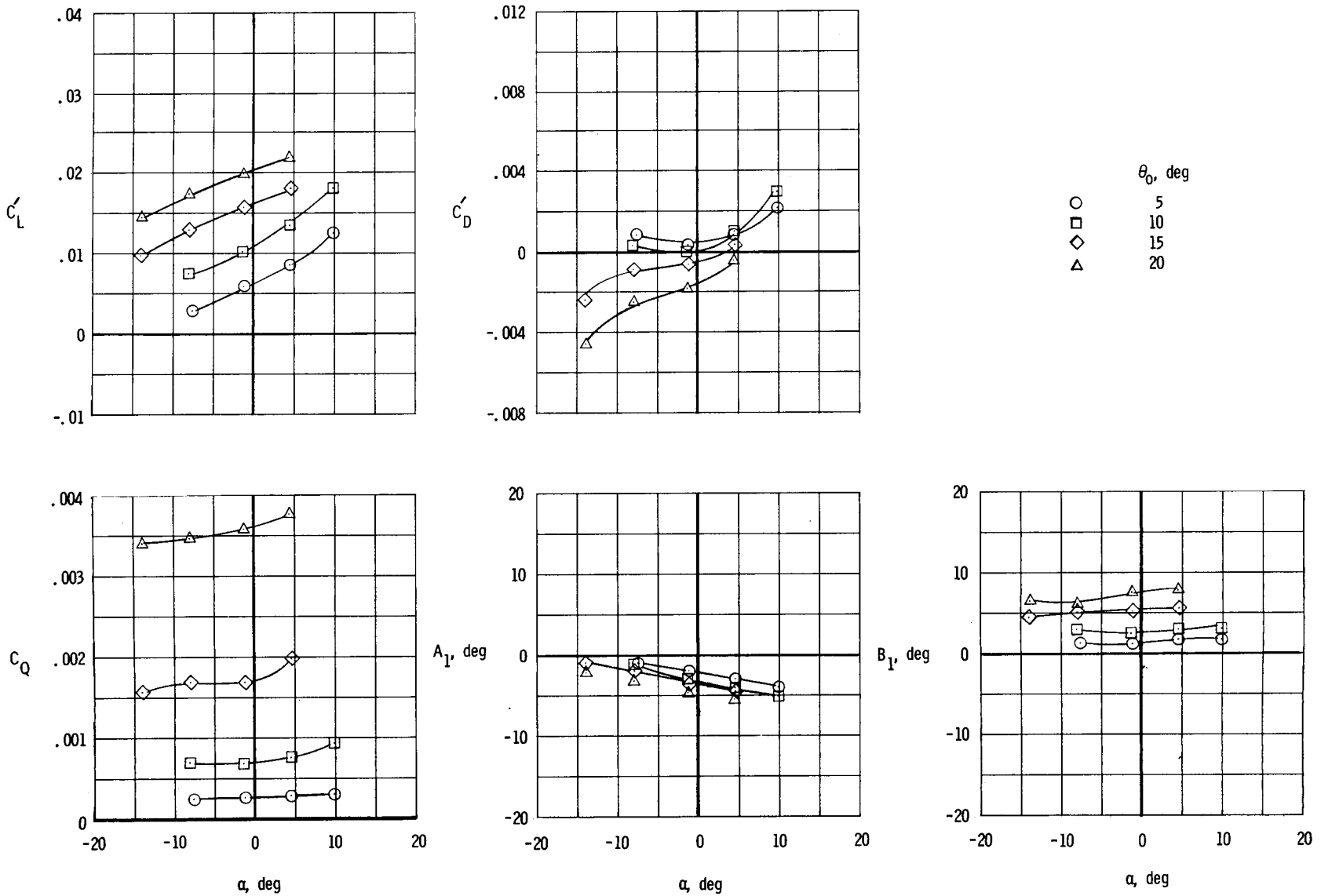

(c) $V/\Omega R = 0.15$.

Figure 12.- Continued.

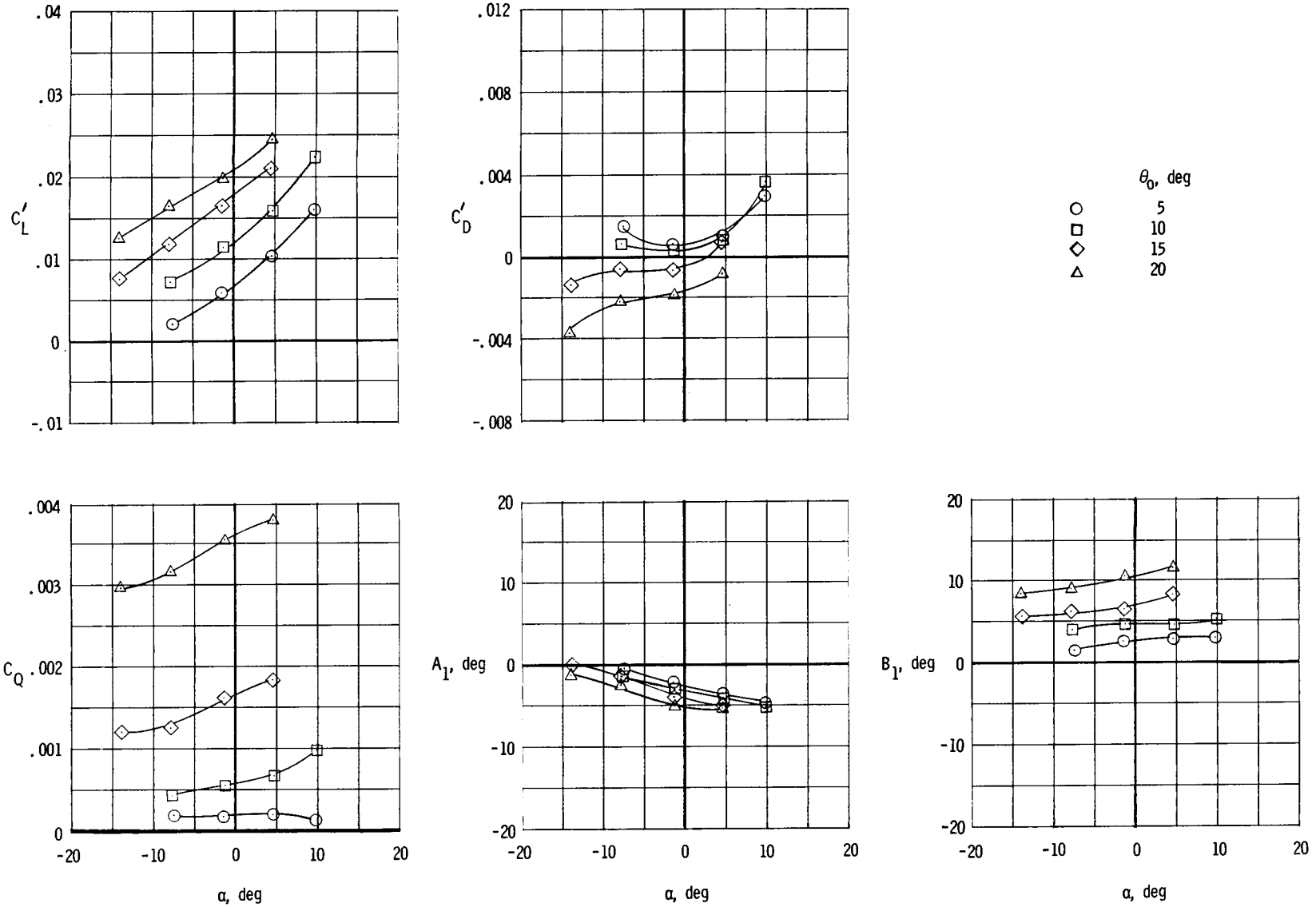

(d) $V/\Omega R = 0.25$.

Figure 12.- Continued.

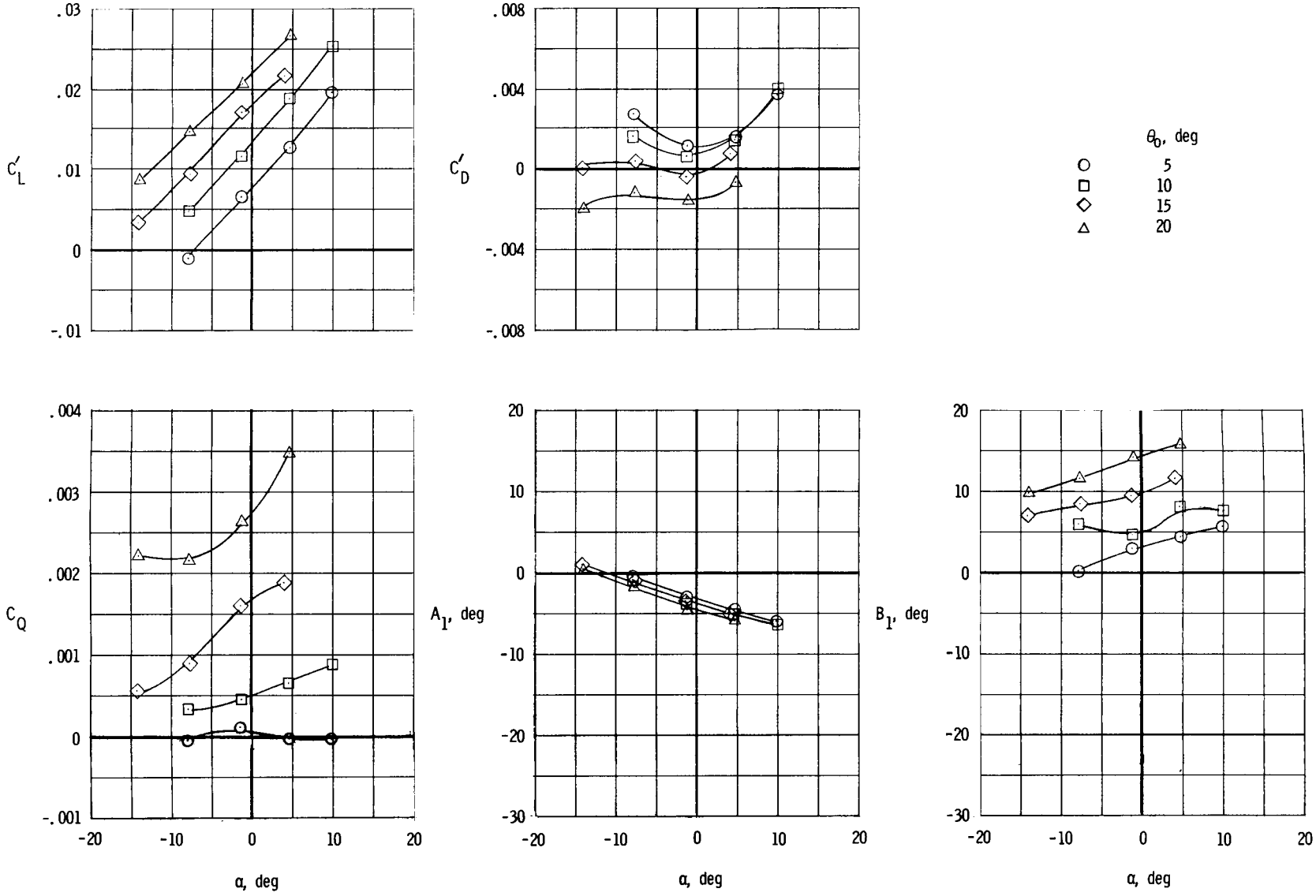

(e) $V/\Omega R = 0.35$.

Figure 12.- Concluded.

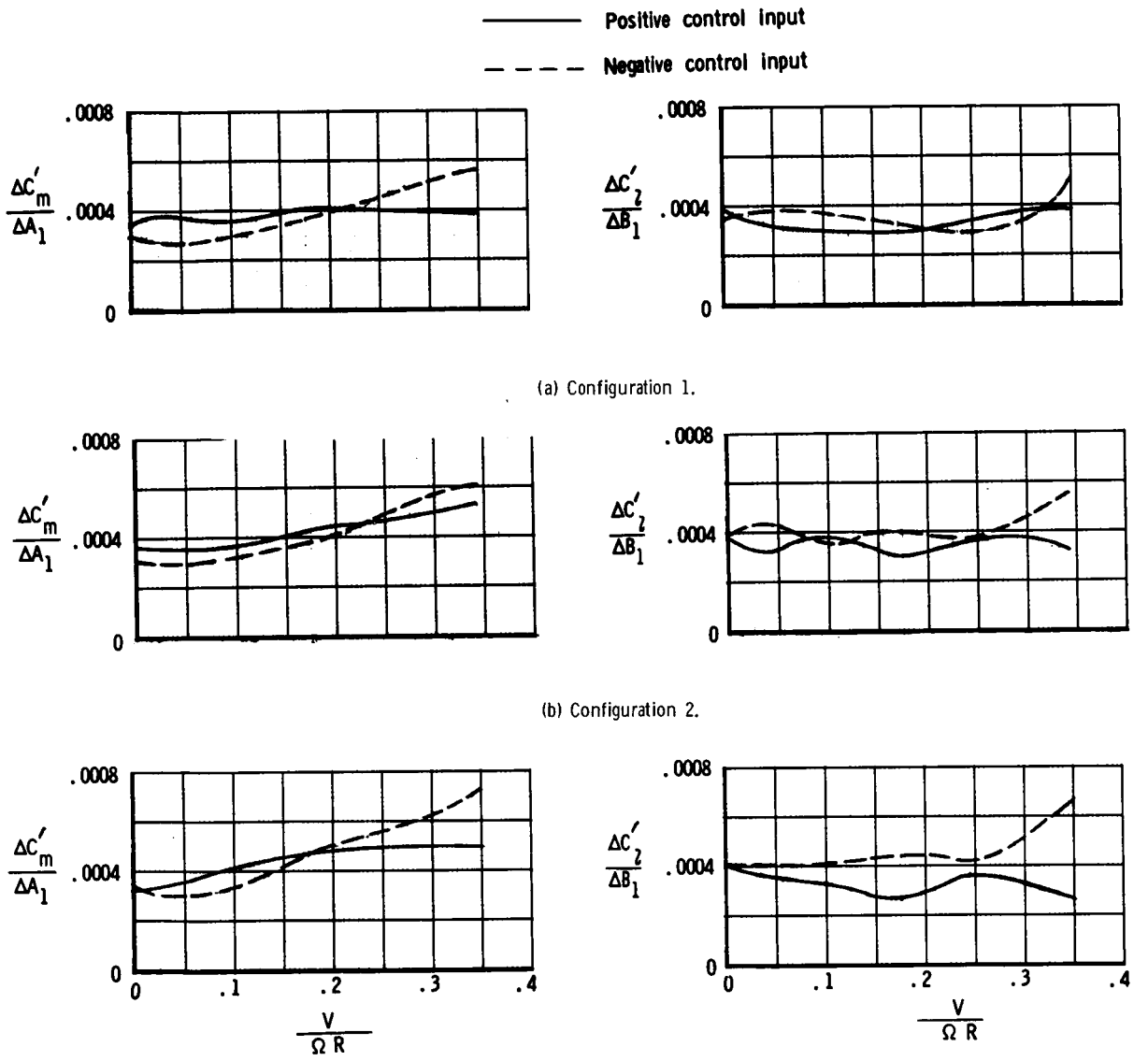

Figure 13.- Variation of cyclic control power with tip-speed ratio for three rotor/wing configurations in helicopter mode. $\theta_0 = 10^0$; $\alpha = -2^0$ (except $\alpha = 0^0$ at $V/\Omega R = 0$).

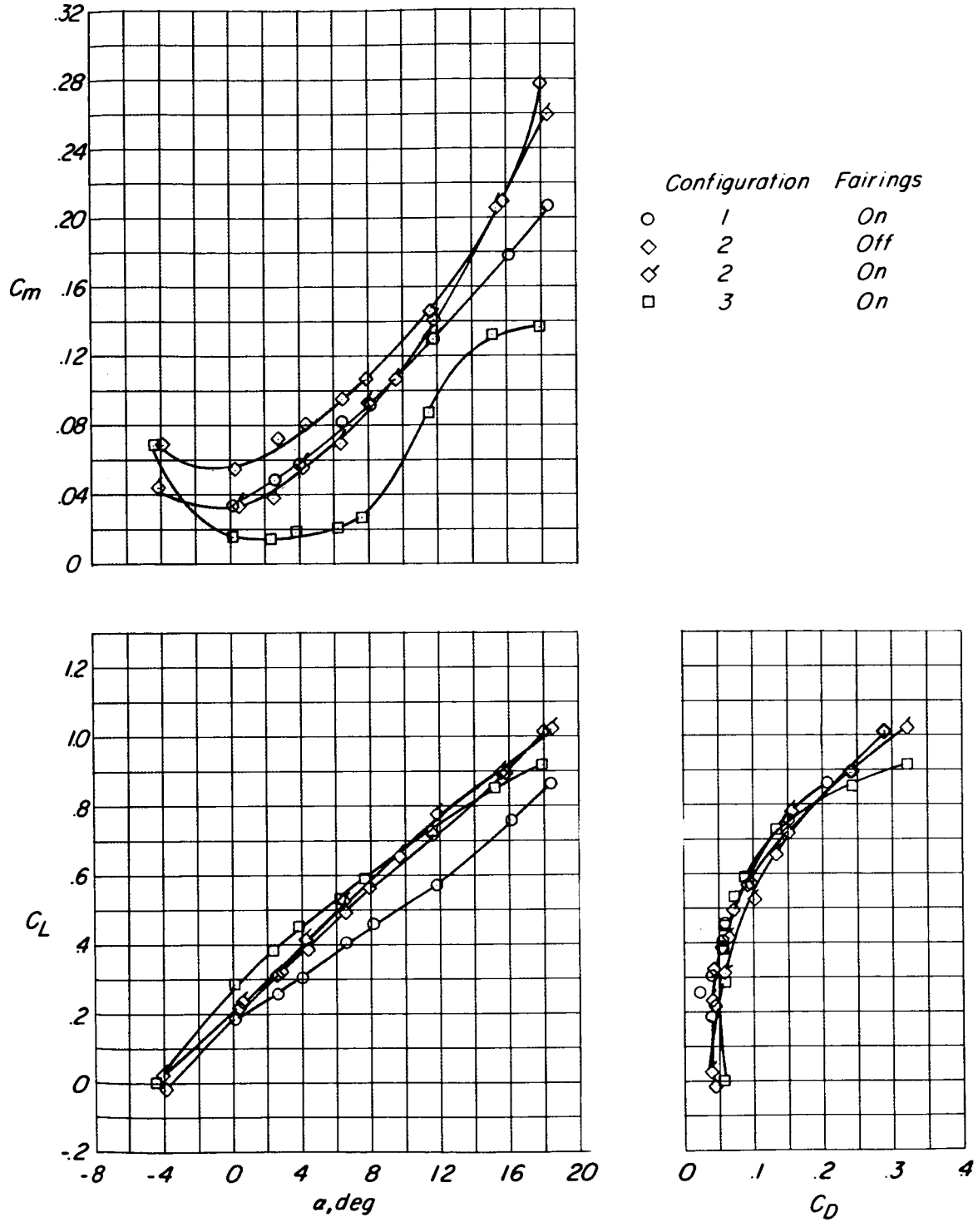

Figure 14.- Longitudinal aerodynamic characteristics of rotor/wing configurations in airplane mode.

NASA-Langley, 1969 —— 2